Detection and Imaging of Underground Structures by Exploiting ELF/VLF Radiowaves

Larry G. Stolarczyk

Raton Technology Research, Inc
848 Clayton Highway
Raton, NM 87740

14 Jan 2000

Final Report

AIR FORCE RESEARCH LABORATORY
Space Vehicles Directorate
29 Randolph Rd
AIR FORCE MATERIEL COMMAND
Hanscom AFB, MA 01731-3010

20020827 003

"This technical report has been reviewed and is approved for publication"

JAMES C. BATTIS
Contract Manager

Gregory P. Ginet
Branch Chief

This report has been reviewed by the ESC Public Affairs Office (PA) and is releasable to the National Technical Information Service (NTIS).

Qualified requestors may obtain additional copies from the Defense Technical Information Center (DTIC). All others should apply to the National Technical Information Service (NTIS).

If your address has changed, if you wish to be removed from the mailing list, or if the addressee is no longer employed by your organization, please notify AFRL/VSIP, 29 Randolph Road, Hanscom AFB, MA 01731-3010. This will assist us in maintaining a current mailing list.

Do not return copies of this report unless contractual obligations or notices on a specific document require that it be returned.

REPORT DOCUMENTATION PAGE

Form Approved
OMB No. 0704-0188

The public reporting burden for this collection of information is estimated to average 1 hour per response, including the time for reviewing instructions, searching existing data sources, gathering and maintaining the data needed, and completing and reviewing the collection of information. Send comments regarding this burden estimate or any other aspect of this collection of information, including suggestions for reducing the burden, to Department of Defense, Washington Headquarters Services, Directorate for Information Operations and Reports (0704-0188), 1215 Jefferson Davis Highway, Suite 1204, Arlington, VA 22202-4302. Respondents should be aware that notwithstanding any other provision of law, no person shall be subject to any penalty for failing to comply with a collection of information if it does not display a currently valid OMB control number.
PLEASE DO NOT RETURN YOUR FORM TO THE ABOVE ADDRESS.

1. REPORT DATE (DD-MM-YYYY) 13 Jan 2000	2. REPORT TYPE Scientific, Final	3. DATES COVERED (From - To) 5 Mar 98-30 Oct 99

4. TITLE AND SUBTITLE
Detection and Imaging of Underground Structures by Exploiting ELF/VLF Radiowaves

5a. CONTRACT NUMBER
F19628-98-C-0012

5b. GRANT NUMBER

5c. PROGRAM ELEMENT NUMBER
63160D

6. AUTHOR(S)
Larry G. Stolarczyk

5d. PROJECT NUMBER
4268

5e. TASK NUMBER
SD

5f. WORK UNIT NUMBER
AC

7. PERFORMING ORGANIZATION NAME(S) AND ADDRESS(ES)
Raton Technology Research
848 Clayton Highway, P.O. Box 428
Raton, NM 87740

8. PERFORMING ORGANIZATION REPORT NUMBER

9. SPONSORING/MONITORING AGENCY NAME(S) AND ADDRESS(ES)
Air Force Research Laboratory/VSBXI
29 Randolph Road
Hanscom AFB, MA 01731-3010

10. SPONSOR/MONITOR'S ACRONYM(S)

11. SPONSOR/MONITOR'S REPORT NUMBER(S)
AFRL-VS-TR-2000-1583

12. DISTRIBUTION/AVAILABILITY STATEMENT
Approved for public release; distribution unlimited

13. SUPPLEMENTARY NOTES

14. ABSTRACT
Clandestime tunnels and underground complexes have been developed in recent years to conceal border crossing passageways and military assets. Ground or airborne attack requires overt and covert imaging to determine the orientation of the underground facility, classification of the overlying rock/soil, burial depth, location of adits, and power and communication lines. Standard worldwide mining practice causes electrical conductors to be installed in the adit and passageways of the underground complex. These electrical conductors form low attenuation rate networks for distribution of EM waves throughout the complex. The electric field component of the primary (illuminating) EM wave induces current flow in these conductors. The current flow causes cylindrically spreading secondary waves to propagate in the surrounding rock mass and become observable on the surface. Mapping the observable provides the information needed for detection. Both analytical codes to determine the underground complex response and highly effective instrumentation for measuring secondary waves have been developed. The High Frequency Active Auroral Research Project transmitter produces and EM wave magnetic field component that is measurable on the earth's surface, making it an effective standoff transmitter for evaluating detection technologies.

15. SUBJECT TERMS
Tunnel detection   Gradiometer
Underground complex
Standoff detection

16. SECURITY CLASSIFICATION OF:			17. LIMITATION OF ABSTRACT	18. NUMBER OF PAGES	19a. NAME OF RESPONSIBLE PERSON James Battis
a. REPORT UNCL	b. ABSTRACT UNCL	c. THIS PAGE UNCL	UNL		19b. TELEPHONE NUMBER (Include area code) 781 377-4669

Standard Form 298 (Rev. 8/98)
Prescribed by ANSI Std. Z39.18

TABLE OF CONTENTS

FIGURES

Detection and Imaging of Underground Structures by Exploiting ELF/VLF Radiowaves
Final Report

FIGURES (CONCLUDED)

EXECUTIVE SUMMARY

Clandestine tunnels and underground complexes (UGCs) have been developed in recent years to conceal border crossing passageways, and military assets. Informants have provided information leading to the capture of eight (8) border crossing tunnels and three (3) tunnels crossing the Korean Demilitarized Zone (DMZ). At the present time, there are two suspect border crossing tunnels under investigation and more than 100 UGCs have been developed by Rogue Nation leaders to conceal military assets. It is currently estimated that over 20 Rogue Nations have constructed underground facilities.[1] Because adits to a tunnel or a UGC must be hidden from surface and high-altitude reconnaissance, deception will always be an important consideration in the construction of these complexes. Ground and airborne attack requires overt and covert imaging technology to determine orientation of the UGC, classification of the overlying rock/soil, burial depth, and location of adits with utilities serving the electrical power and communication needs. To be effective, the technology must provide this information in real time.

Although the detection and imaging of tunnels and UGC is a tough science and engineering problem, it is not an intractable problem. A series of analytical investigations and associated field tests has increased our understanding of how primary electromagnetic (EM) waves interact with the underground infrastructure and create secondary EM waves that are observable on the earth's surface. The evolution of active EM detection and imaging technology begins with our development of EM technology for the mining industry. For many reasons, the worldwide mining industry has developed a standard practice of installing electrical conductors in the adit and passageways of the UGC. Clandestine tunnels and UGCs will most likely use this well-established practice. Our work in developing mine-wide radio communications equipment has

shown that the electrical conductors in the underground passageways form a low attenuation rate network (waveguide) for distribution of EM waves throughout the complex. It is the electric field component of the primary (illuminating) EM wave that induces current flow in these conductors.

The current flow causes cylindrically spreading secondary waves (decay with the one-half power of distance from the conductor) to propagate in the surrounding rock mass and become observable on the surface. Mapping the observable provides information for determining the orientation of the infrastructure, burial depth, and the location of the active adit. The resistivity of the overlying material can be determined from these measurements enabling the classification of rock mass overlying the UGC. Evolution in our understanding of active EM has resulted in the development of analytical codes for determining UGC response and highly effective instrumentation for measuring secondary waves.

The High-Frequency Active Aurora Research Project (HAARP) transmitter low frequency modulation of the electrojet produces an EM wave magnetic field component that is measurable on the earth's surface. The HAARP transmitter is an effective standoff source for evaluating and optimizing active EM clandestine tunnel and UGC detection and imaging technologies. The engineering challenge is the development of instrumentation that can measure *in real time* the tunnel and UGC response due to EM waves with magnetic field components in the picoTesla range (Tesla = Weber per square meter). Such instrumentation would also enable the measurement of EM waves from other opportunistic standoff sources. These sources cause EM waves to propagate in the earth-ionosphere waveguide to the target area causing an observable scattered EM wave from the UGC. To meet the engineering challenge in this project, instrumentation featuring synchronous detection and a gradiometer antenna array were

developed and evaluated in a series of field tests. Research has shown that the optimum detector in the sense of maximizing the receiver threshold sensitivity for continuous wave (CW) signals is achieved with synchronous detection.[2] Synchronous detection requires that a separate receiver channel be built into the gradiometer receiver design for reception and synchronization with the primary wave illuminating the tunnel and UGC. The advantage of the EM gradiometer antenna array (sometimes referred to as Resonant Electromagnetic Gradiometer Array [REMGA]) is that a CW signal like the primary HAARP EM wave and other standoff sources is suppressed while the scattered secondary EM wave causes a response from the UGC.

The synchronized EM gradiometer instrument was built and field data were collected and analyzed from four (4) different test sites. Testing at the National Rifle Association (NRA) Whittington Center near Raton, New Mexico, determined that the burial depth could be determined from the gradiometer receiver data. The Otay Mesa drug smuggling tunnel near San Diego, California, provided an opportunity for evaluating the gradiometer response that showed that the center line and burial depth could be determined from the acquired data. The Silver Fox and Permafrost tunnels provided yet another opportunity of evaluating the gradiometer response. This report describes the science and engineering principles underlying the synchronized EM gradiometer instrument design and field data acquisition results.

1. BACKGROUND INFORMATION

The development of a UGC begins with the application of underground mining practice. There are a small number of highly regarded academic institutions that educate and train mining engineers, geologists, and geophysicists. The curriculum and textbooks are very similar in these institutions. The mining community is drawn together (networking) by trade associations and

national/international trade shows/conferences. Technical specialization includes mine design, ground control, ventilation/drainage, electrical design, conveyance/transportation, and geology/geophysics. Standardization in mining practice is nurtured by the health and safety regulations that propagate worldwide from basic lessons learned in mine disasters. Causing further standardization in mining practice is the propensity of some foreign governments to provide incentive to equipment manufacturers in developing machinery for the worldwide mining market. A mining machine that is proven to be reliable will be sold and "standardized" throughout the world. Mines in developing countries and in similar geology employ the same practice and mining equipment. A typical underground facility is illustrated in Figure 1.
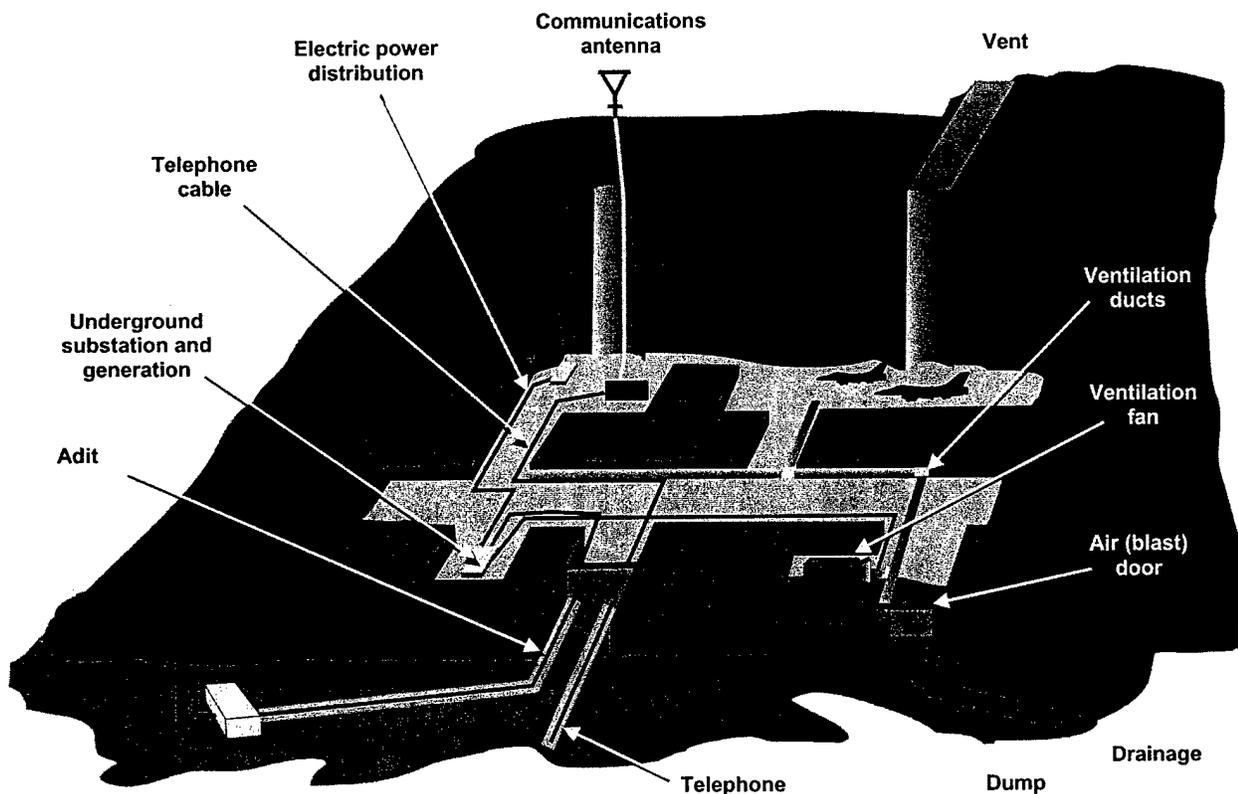
Figure 1. Typical underground facility

The detection and defeat of clandestine tunnels and Rogue Nation UGCs depends on our knowledge of standard mining practice. The underground infrastructure that results from standard mining practice creates the observables upon which close-in and standoff detection and imaging technologies are based.

2. MINE DESIGN

The development of geologic models begins with field studies of surface features and outcrops. The geologic information base is oftentimes expanded by mineralogical evaluation of cutting and core. The data set may include a suite of borehole logs. From these data, a model of the prevailing geology is developed. Based upon the geologic model, mining engineers develop the extraction plan and specify the mining equipment. The mining plan includes specifications for ground control, ventilation, muck transportation, drainage, and power/telephone system.

2.1 Ground Control

The theory and practice are discussed in technical meetings such as the recent 18th International Conference on Ground Control in Mining held at West Virginia University (WVU), the Society of Mining Engineering annual meetings (March 1 in Salt Lake City), and the National Mining Association (NMA) International meeting MinEXPO 2000 (October 2000).

2.2 Description of Observables

In cut-and-fill structures, roof support will be designed to support the overlying fill material. Besides the observable disruption of vegetation, the structures will include steel support beams and steel mats (metal screens) that are EM observable.

The Cloud Chamber at the Department of Energy (DOE) Nevada Test Site (NTS) is a good example of a cut-and-fill site. It is constructed with steel arch supports. The structure includes

shallowly buried electrical conductors that served the scientific purpose of the nearby underground nuclear test. EM wave sources easily induce current flow in these umbilical conductors. The magnetic anomaly is extremely large and causes a hand-held compass to deviate over the structure.

Drug smuggling tunnels developed in the Nogales, Arizona, area collapse without aggressive ground control measures.

Structures developed into hard rock have similar ground control requirements. At the adit, weathering causes the ground to be incompetent. Aggressive use of steel/wood supports along with metal screening is required. Reinforced concrete is oftentimes used in the construction of an adit. As the entries are developed, ground control measures intensify with strata depth. The ground control measures also increase with the width of the entry. EM waves induce current flow in reinforced concrete.

The Korean DMZ simulation tunnel at the Colorado School of Mines (CSM) Idaho Springs experimental mine was driven into a schist. The ground control included use of roof bolts. Where the development entry crossed a fault, the ground control measures were intensified to include metal screening on the back (roof). The ground control measures are similar at many of the NTS tunnels.

The WVU 18th International Conference on Ground Control in Mining included a number of papers that provided statistical data on roof failure over time. Roof failure occurs frequently resulting in rock fall; each fall becomes a seismic event. An array of geophones (microseismic technology) has become standard practice in many mines. The microseismic method can be developed for location of passageways in a UGC.

Drill-and-blast extraction predominates in hard rock entry development. Removal of fragmented materials requires muck-handling vehicles. Rail and muck cars are a preferred transportation method. Because of the heat released with electric-powered drills, pneumatic drills are preferred because they cool the working face and improve ventilation. High-pressure air pipes are designed into the mine infrastructure.

Blasting creates seismic events. Rails and high-pressure air pipe installed throughout the UGC can be mapped by measuring scattered EM waves from electrical conductors.

During the US Army campaign against the Korean DMZ tunnels, intelligence provided information on suspect tunnel locations. The information included the fact that the tunnel boring machines (TBM) had been exported to North Korea. TBM boring creates unique acoustic signals. None of the discovered DMZ tunnels were built with TBMs. These machines must be used elsewhere in North Korea. The first shallow-buried DMZ tunnel was detected by observation of anomalous snow melt along the center line of the tunnel. This tunnel should be classified in the cut-and-fill category because of the wood support ground control measures used in building the tunnel. Tunnels 2, 3, and 4 were driven into schist with drill-and-blast methods. Evidence in the captured tunnel suggests that rail was used to transport muck. Lighting brackets were also observed on the ribs (walls) of the tunnel.

The NTS Yucca Mountain Tunnel was developed with a TBM. The reinforced concrete and extensive electrical cable become EM observables.

2.3 Ventilation/Drainage

Mining engineers know that water will most likely be encountered in developing entries. The DMZ and Otay Mesa tunnels were developed upgrade (approximately 1½ degrees) so as to

dewater the mine. Mine drainage water will most likely exit the suspect UGC at the adit. In sulfide-bearing rock mass, the drainage water will be acidic, causing discoloration in the surface soil and retardation in vegetation.

Bacteria play a significant role in mine ventilation. When sufficient oxygen is present, the relatively warm and moist underground environment fosters rapid accumulation of aerobic bacteria strains. Carbon dioxide (black damp) builds up in unventilated areas. In oxygen-deficient tunnels, anaerobic bacteria strains rapidly accumulate. Septic conditions result in the release of hydrogen sulfide and methane.

Mine ventilation conferences are periodically held and attract mine personnel from all over the world. Ventilation engineers discuss resistive analog models to characterize fresh-air flow throughout the mining complex. Fans, air ducting (tubing), and regulators are simulated in the analog model and then deployed so as to drive fresh air through the entries and into the working areas. The primary fan is located as near the adit as possible. An air door is oftentimes used to cause overpressure in the mining complex and force the exhaust air to exit through the vents developed at the extreme end of the

Figure 2. Silver Fox Mine tunnel with rail and ventilation

complex. An adit air door is not required in some mines. Air ducts convey fresh air to the working area and the air returns to the adit in the passageway. The ventilation system may also be designed around an exhaust fan system. Ventilation tubing includes electrically conductive spiral wire (Figure 2). Induced current flow is an observable in the active EM detection method.

Fans require electric power. Large underground mines have difficulty in maintaining adequate ventilation. Oftentimes a system of smaller fans is deployed in working areas to increase air flow.

Three-phase electric power is required for the main fan. Main fans in remote locations are oftentimes diesel/propane powered. The system of smaller fans is connected to single-phase power. These cables become observables with EM methods.

Mine fires typically advance in the direction of the fresh-air source (called an intake). This fact may become an observable during an attack. Carbon monoxide monitors are used to detect incipient mine fires. Monitoring of the vent for gas composition with a LIDAR will be an effective means to determine status prior to, during, and after attack.

It should be noted that non-toxic "stench" gas is injected into the ventilation system to notify mine personnel of an emergency condition. Personnel evacuate the mine along designated escape ways. Tracer gas may be deployed during an attack at the adits and then monitoring can be used to locate exhaust vents.

2.4 Electrical/Telephone Design

The electrical/telephone design practice is highly dependent upon the worldwide health and safety standards/regulations. These standards are different for gassy and non-gassy mines.

In Third World countries, three-phase wires enter the complex and then three separate conductors run along the rib (side) of the drift. This occurs because three-phase cables are too expensive and difficult to obtain in these countries. These conductors support low attenuation rate monofilar and bifilar EM wave propagation in the mine. Since these conductors traverse

most of the mine entries, induced current flow and the resulting secondary waves become observables in determining the orientation of entries in the UGC.

In non-gassy mines, electrical transformers and switches are designed to surface standards. However, in gassy mines, flameproof enclosures are designed around these electrical apparatus.

Electrical grounding is an exceedingly important aspect in electrical design. Because a common motor failure mode is the phase winding becoming shorted to the motor frame, the frame will be at phase voltage of the power system. Electrocutions often occur because it is difficult to maintain a continuous grounding conductor throughout the mine. When the ground conductor fails (rock fall or improper repair), the main substation safety circuit breaker will not switch when the motor grounding condition occurs. Therefore, the mine electrical grounding system requires special consideration in mine electric power system design.

Because of grounding requirements, a dedicated conductor must run throughout the mine. Mining machinery induces a unique current flow in this conductor; it becomes an EM observable. For example, induction motors during start-up cause a triangular-shaped ground current to flow. The Fourier series representation of induced current includes odd harmonics that decay as the inverse square of the odd harmonic number. There is also a strong component at the induction motor slip frequency. By monitoring the slip frequency, motor loading can be determined. Three-phase rectifiers create strong harmonics that decay as the inverse first power of the harmonic number. In general, below 100 kHz the mine-generated electrical noise density spectrum increases as the inverse power of frequency.

3. SCIENCE AND ENGINEERING HISTORY OF ACTIVE EM DETECTION AND IMAGING

The United States' scientific interest in a capability to detect clandestine tunnels and UGCs began during the Vietnam War. The interest was intensified by two post-Vietnam events: discovery of tunneling under the US Embassy in Moscow and the discovery of North Korean tunneling through the DMZ. The US Army Belvoir Research and Development Engineering Center (BRDEC) conducted tunnel-detection science and engineering investigations in support of the US and South Korean armies' campaign against the DMZ tunnel threat. The science and engineering investigations were reported in several conferences sponsored by BRDEC. The initial design of the EM gradiometer instrumentation grew out of the BRDEC program. The discovery (1992) of the Otay Mesa drug smuggling tunnel near San Diego, California, occurred as the funding for the DMZ campaign was terminated. The timing of the Otay Mesa tunnel discovery provided an opportunity for the experienced BRDEC program personnel to compare various geophysical techniques against this target. The BRDEC (1993) report on the Otay Mesa campaign found that "to be successful in detecting/locating a tunnel or a cavity requires combining the use of high-resolution geophysical techniques having good depth of penetration with advanced signal processing and interpretation techniques."[3]

One of the conclusions of the BRDEC study was that active frequency-domain (continuous wave) electromagnetic-gradiometer imaging systems clearly demonstrated the capability to detect and define the Otay Mesa Tunnel.[4] While the tunnel conductors provided the strongest target, the survey also demonstrated that a tunnel without conductors can be detected with high-frequency (15 MHz) cross-borehole instrumentation. Ground penetrating radar (GPR) operating at frequencies above 20 MHz was not able to detect the tunnel.

In 1994, a panel of DOE National Laboratory geophysicists accepted an assignment to assess the state of the geophysical technologies that might be applied in the underground structures detection problem. The DOE/NN-20 Program (Benchmark Study, 1994)[5] resulted from this work. Sandia National Laboratories (SNL) focused on the low-frequency EM gradiometer work originally developed in the BRDEC program. A laboratory (not a prototype) EM gradiometer design very similar to the original Otay Mesa instrument was built and field data collected with this instrument.[6] The laboratory EM gradiometer instrument design required that an umbilical cable be connected between the transmitter (source) and the EM gradiometer receiver. Although the instrument was successful in detecting underground targets at the Nevada Test Site (NTS), it was cumbersome to use in the field. The primary goal of this project was to eliminate the need for an umbilical cable by causing the EM gradiometer receiver to be self-synchronized with the EM wave illuminating the surface overlying the clandestine tunnel or UGC. A second goal was to dramatically increase the EM gradiometer receiver threshold detection sensitivity so that the HAARP signals in the picoTesla range could be used in detection and imaging of UGC. These synchronized EM gradiometer receiver enhancements would enable the use of opportunistic standoff transmitters prior to and during military operations when access is denied.

The science of EM detection and imaging of clandestine tunnels and UGCs is based upon the induction of current in passageway electrical conductors and reinforced concrete.

Harrington [7] developed a simple formula for the induced current (I) in long, thin electrical conductors when illuminated by the electric field component (E) of the EM wave. The total current (I) is given by

$$I = \frac{2\pi E}{i\omega\mu \log ka} \qquad (1)$$

where $\omega = 2\pi f$ and f is the frequency in Hertz of the primary EM wave,

$\mu = \mu_o\mu_r$ is the magnetic permeability of the surrounding rock mass, $\mu_o = 4\pi \times 10^{-7}$ farads per meter and $u_r = 1$ in most natural media,

k = β-iα is the wave propagation constant where β is the phase constant and α is the attenuation rate, and

a is the radius of the conductor in meters.

This is one of the fundamental equations that is applied in the active EM method of tunnel and UGC detection. For a thin electrical conductor in a tunnel, the equation teaches that the induced current increases with the amplitude of primary EM wave electric field component that is tangential to the electrical conductor and inversely with frequency (ω). Therefore, lower frequency EM waves are preferable and compatible with the HAARP transmitter electrojet modulation capability and other standoff opportunistic sources that utilize the earth-ionosphere waveguide. Actual measurements conducted at the Colorado School of Mines (CSM) BRDEC tunnel proved that the induced current as defined in Equation (1) increased as frequency decreased.[8] For a magnetic dipole source, the longitudinal electric field component is given by

$$E_\phi = \frac{i\mu\omega M k^2}{4\pi}\left[\frac{-1}{(kr)^2} + \frac{1}{i(kr)}\right]e^{-ikr}\sin\phi \qquad (2)$$

where M = NIA is the magnetic moment (turn peak ampere square meters), and

ϕ is azimuthal angle in degrees.

Because of the ω term in the above equation, the electric field vanishes at zero frequency; therefore, for magnetic dipole sources there is an optimum frequency for inducing maximum current. Primary EM waves that propagate as earth-ionosphere waveguide signals are quasi

transverse EM waves (TEM), which produce uniform illumination of the clandestine tunnel and UGC target area. In the case of a waveguide TEM wave, the magnitude of the electric field is not frequency dependent as in the case of the magnetic dipole source.

Harrington goes on in his formulation to show that the secondary EM wave scattered from the electrical conductor will slowly decay with distance from the conductor at radial distances that are large compared with the skin depth (see Figure 6). Burrows [9] also develops similar formulations as

$$H_s = -\phi \frac{i l_s k}{4} H_1^{(2)}(kr) \tag{3}$$

and

$$Es = -Z \frac{\omega \mu I}{4} H_0^{(2)}(kr) \tag{4}$$

where ϕ, Z are unit vectors,

$H_o^{(2)}$, $H_1^{(2)}$ are Hankel functions of the second kind (order 0 and 1),

and   r is the radial distance in meters to the measurement point.

At radial distances that are large compared with the skin depth, the asymptotic formula of the Hankel function leads to simplified expressions:

$$Hs \approx \Phi \frac{Is}{2} \left(\frac{ik}{2\pi r} \right)^{\frac{1}{2}} e^{-ikr} \tag{5}$$

and

$$Es \approx -Z \frac{\omega \mu \, Is}{2} \left(\frac{i}{2\pi kr} \right)^{\frac{1}{2}} e^{-ikr}. \tag{6}$$

The secondary cylindrically spreading EM waves decay with the half power of distance (r) from the conductor. They are decreased in magnitude by the attenuation factor $e^{-\alpha r}$. A gradiometer antenna is designed to measure the gradient of the cylindrically spreading EM wave. The reception of secondary EM waves in the rock mass surrounding the tunnel or on the surface confirms the existence of nearby electrical conductors.

David Hill reformulated the problem for finite length conductors and non-uniform illumination by a magnetic dipole source.[10] In this case, standing waves occur on the underground conductors. In a passageway with multiple conductors, the standing wave pattern is *not* observable because of multiple reflections in the ensemble of electrical conductors.[11]

Bartel and Cress used forward modeling codes developed by Gregory Newman to show that current flow is induced in reinforced concrete.[6] Forward modeling codes are now available to determine UGC response for EM sources above and below the earth's surface.[12]

Wait and Hill have theoretically shown that the passageway conductors form low attenuation rate transmission networks (waveguides) for distribution of induced current throughout the UGC.[13]

Figure 3 shows that the attenuation rate is less than 1.0 dB per kilometer at 50 kHz.
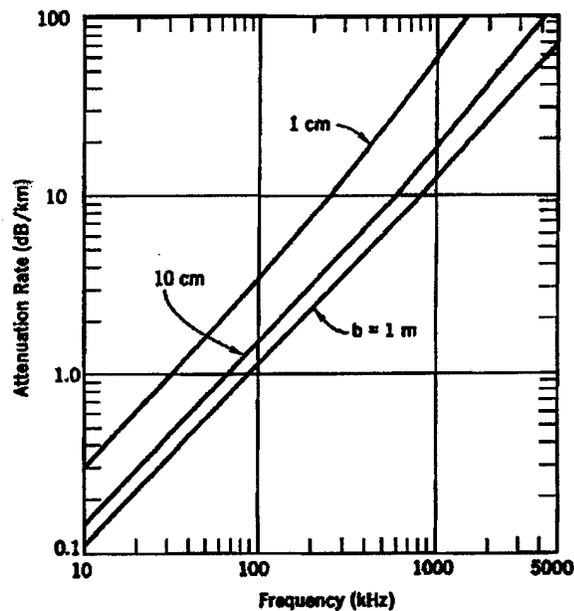

Figure 3. *Conductor mode attenuation rate versus frequency for conductor to rock mass air path distance of 1 cm, 10 cm, and 1 m (after Hill [13])*

The current appears on the electric power and telephone cables entering the complex through the adit. Because of grounding conductors, switches will not disrupt current flow. Switch and transformers add attenuation to the signal.

Hill has formulated the problem of measuring the gradiometer response to induced current flow in a passageway conductor.[14][15] The gradiometer response is shown in Figure 4.

The total field shown on the right is the sum of the primary and secondary field. The gradient of the total field is shown on the left. Whereas the total field changes by only a few percent, the gradient changes by tens of percent when the gradiometer passes by the conductor.

When quasi-TEM earth-ionosphere waveguide signals are used, EM waves couple across the air-soil boundary and propagate downward. The attenuation rate (α) and phase shift (β) values are shown in graphical form in Figure 5.
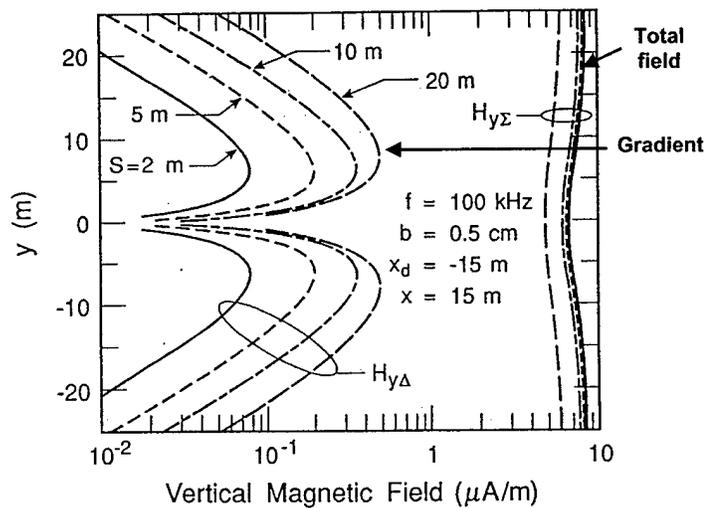
Figure 4. *Gradiometer response to current flow for various gradiometer dipole spacings (after Hill [14]) conductor located at y = 0 and directed into the page*
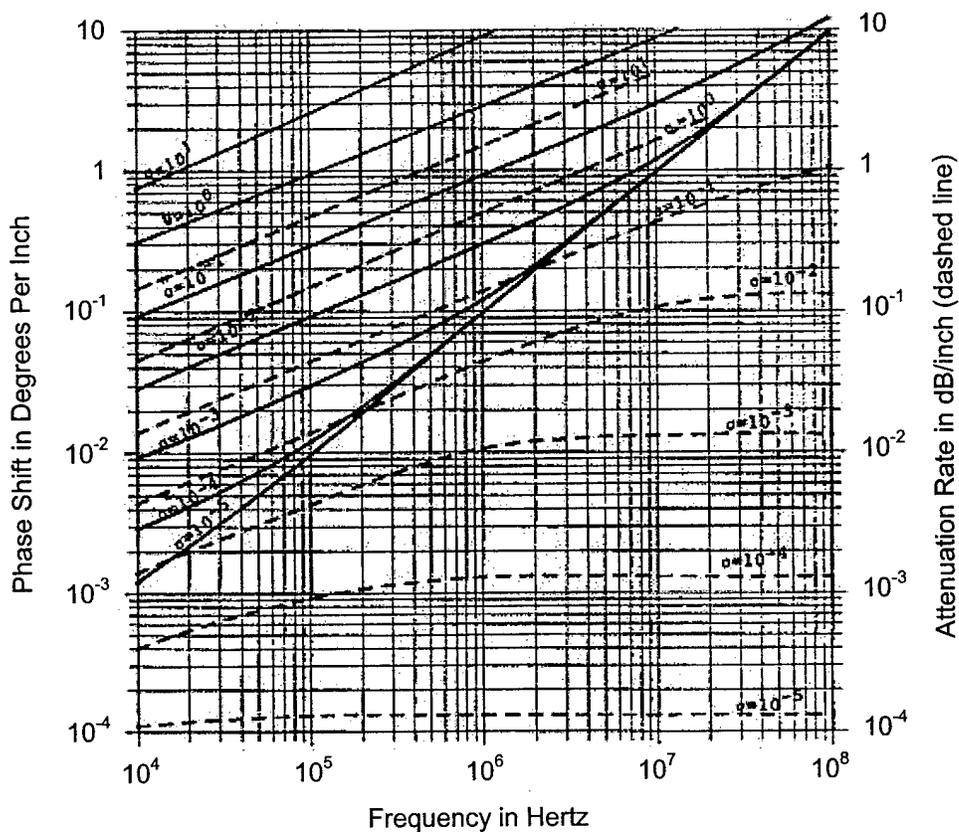
Figure 5. *Attenuation rate (α) and phase constant (β) for a uniform plane wave propagating in natural medium with a relative dielectric constant of 10. The bottom-to-top curves represent increase in natural media conductivity from 10^{-5} to 10^{1} S/m. For completeness, the skin depth and wavelength of subsurface EM waves are shown in Figure 6.*

Figure 6. *Skin depth and wavelength in a natural media with relative dielectric constant of 10*

The propagation constant can be estimated for various types of natural media using the data

in Figure 7 below.

Figure 7. *Range of electrical conductivity and relative dielectric constant for natural media*

It is important to realize that the electrical conductivity of most natural media increases with frequency. The left end of the bar symbol in Figure 7 corresponds to low frequency values. Figure 5 shows that the lower frequency signal attenuation rat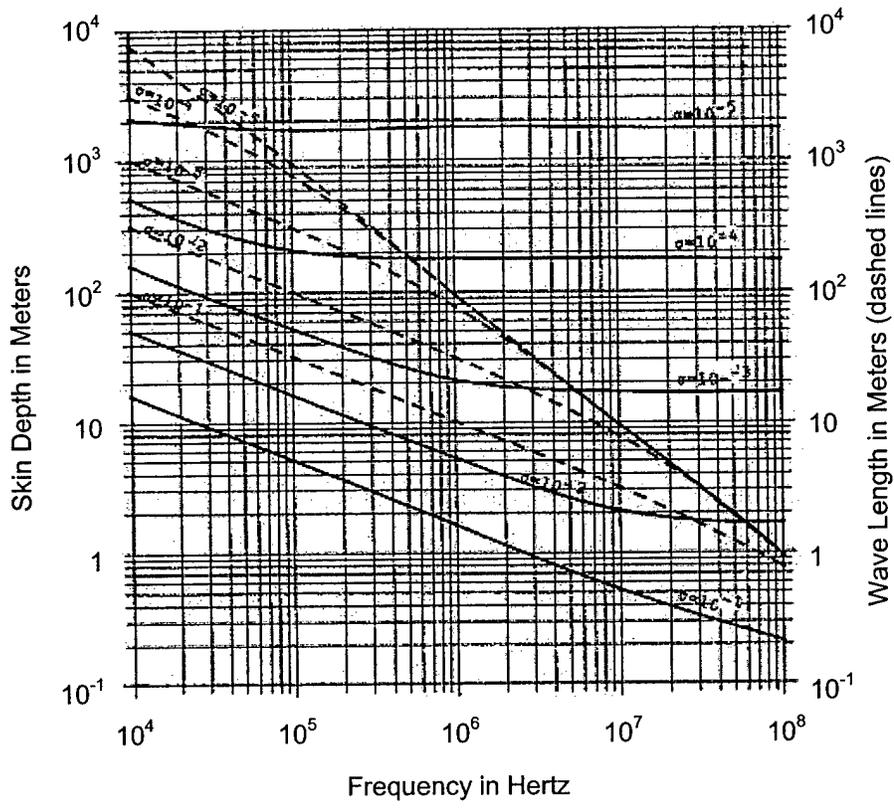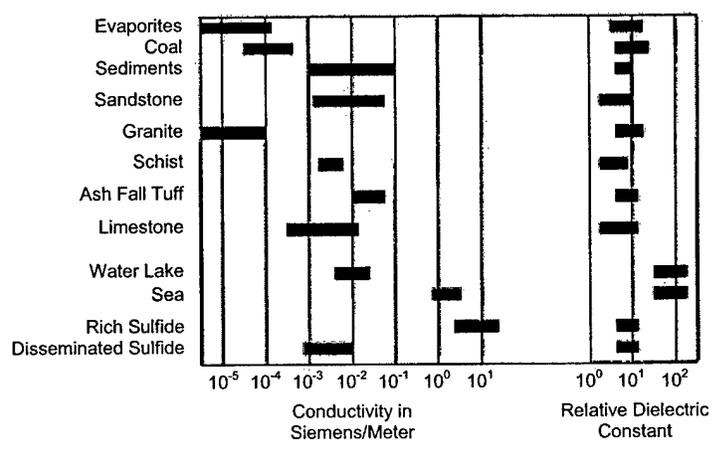e decreases from high frequency values so that deeper targets are detected at lower frequencies. All too often, GPR technologies are proposed for the UGC problem. At 100 MHz (in a 10^{-1} S/m media), the attenuation rate is approximately 39 dB per meter and prevents receiving an observable at this frequency on the surface. This was confirmed in the BRDEC campaign against the Otay Mesa drug smuggling tunnel.[3]

One advantage of the gradiometer is that it can be used on the surface. Radiowave interference from distant sources will be plane waves and suppressed by a gradiometer antenna. The gradiometer measurement of tunnel and UGC response exhibits a high signal-to-noise (S/N) ratio—favorable for reducing the false alarm rate (FAR).

During the DOE underground structures detection program, Bartel and Cress demonstrated that EM gradiometer receivers could detect scattered secondary waves from the USGS seismology vault near Kirtland Air Force Base (KAFB), the Cloud Chamber at the NTS, and the Yucca Mountain Tunnel.[6] The seismology vault near KAFB was developed into a granite outcrop. The response to the reinforced concrete and electrical power cables is shown in Figure 8.
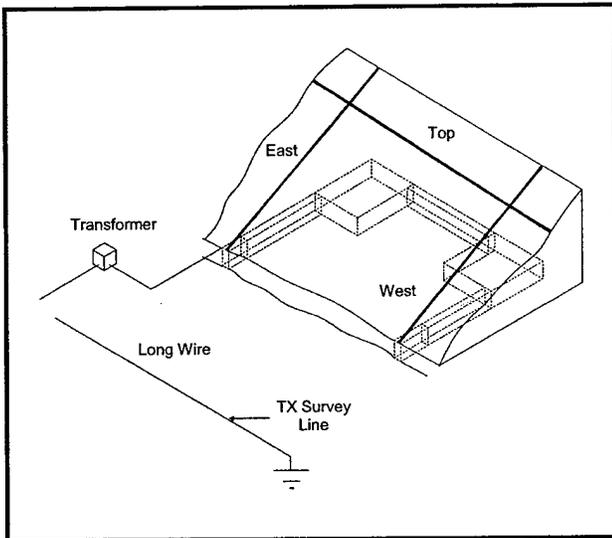
Pictorial view of seismology vault and survey lines
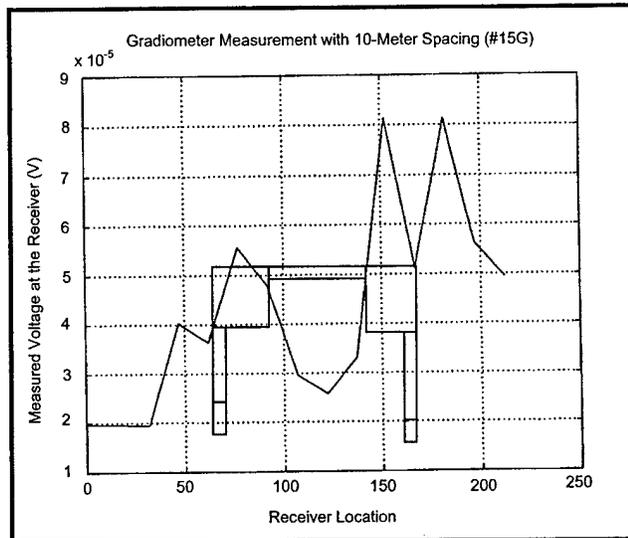
Top scan line gradiometer response at 102.5 kHz. VMD source is located at power center.

Figure 8. *Seismology vault near Kirtland Air Force Base*

The engineering of EM gradiometer instrumentation is driven by the very small magnitude of the HAARP electrojet signal measured on the earth's surface. The measured ionospheric signal is shown in Figure 9.

The spectrum exhibits minimum values in several frequency bands. The HAARP research projects have generated signals below 1 kHz where the electrojet
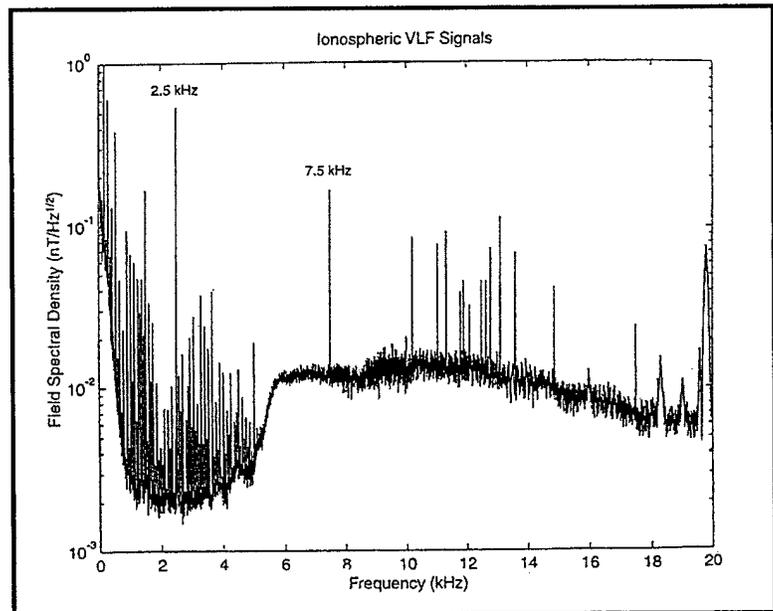

Figure 9. *Ionospheric VLF noise spectrum*

signals are measured in the picoTesla (Tesla = Weber per square meter) range. A gradiometer designed to operate in the 9-kHz frequency range would operate in a noise field of approximately

2.0 x 10^{-2} picoTesla per square root Hertz. The expected S/N ratio would be $1 \div 2$ x $10^{-2} = 50$ (34 dB). The spectrum also exhibits strong discrete components that must be discriminated against (by filtering) in the EM gradiometer receiver design.

Middleton describes signal detection processes that are optimum in the sense of maximizing receiver threshold detection sensitivity.[2] For a sinusoidal signal embedded in white electrical noise, synchronous detection maximizes the threshold detection sensitivity. The receiver detection sensitivity is given by

$$S_T^{10} = -164 + 10 \log_{10} BW + 10 \log_{10} NF \quad dBM \qquad (7)$$

where BW is the noise bandwidth of the receiver in Hertz, and

      NF   is the noise figure of the receiver.

The received signal S_T^{10} produces a 10-dB S/N ratio in the receiver signal path. The first right-hand term (-164 dBM) represents a signal of 1.41 nanovolts that produces a S/N ratio of 10 dB in the receiver signal path. The far right-hand term represents the threshold detection sensitivity degradation due to receiver noise figure. Typically, a well-designed receiver will exhibit a noise figure near 2 dB. The middle term shows that the noise bandwidth (BN) is the predominating factor in the receiver design problem.

The receiver threshold sensitivity increases as bandwidth is reduced. By synchronizing the receiver to the EM wave illuminating the target, the receiver bandwidth can be made very small. Alternatively, a wider bandwidth can be used in the design where sampling and averaging can be used to achieve narrow effective bandwidth; however, this type of system would not be able to discriminate against the discrete spectrum shown in Figure 9.

Detection and Imaging of Underground Structures by Exploiting ELF/VLF Radiowaves
Final Report
RTR-2000-01   Page 21

4. SYNCHRONIZED EM GRADIOMETER

A simplified block diagram of the synchronized EM gradiometer instrumentation is

illustrated in Figure 10.
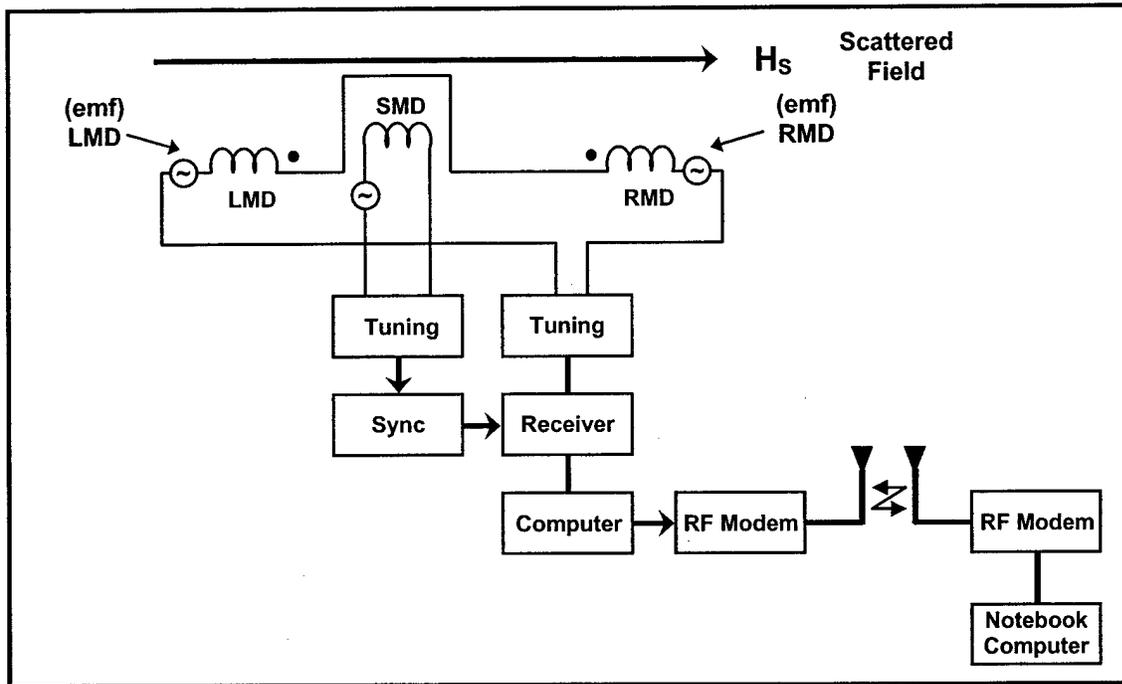
Figure 10. EM gradiometer instrumentation block diagram

The gradiometer antenna array consists of two ferrite-core magnetic dipole antennas (LMD

and RMD) electrically coupled and 180 degrees out of phase. This is called the differential mode

of operation. For maximum primary wave cancellation the antennas are coaxial (antenna rod

axes along same axis) and paced on a base line perpendicular to the intended target's trend. The

magnetic dipole antennas may also be connected in the summation mode of operation. In this

case, the instrument would not operate as a gradiometer, but as a single magnetic dipole. The

LMD and RMD antenna may be configured as vertical or horizontal magnetic dipoles. During

the field tests to be described later, the horizontal magnetic dipole configuration was used. The

instrumentation consists of a central electronics enclosure and telescoping antenna assembly

enclosed in fiberglass. The antenna assembly tubing also has a center section containing the synchronization and calibration antenna (SMD). Measured data are transmitted to the remote laptop computer via an RF-modem in the enclosure. The system maintains operation for 6 hours on a single lead-acid rechargeable battery. The gradiometer receiver is carried by an operator using a belt and shoulder strap.

The data are recorded by a laptop computer for later reduction and graphing. The computer operator must be within a quarter mile of the receiver (less in forested areas).

The block diagram of the EM gradiometer receiver developed in this work is illustrated in Figure 11.

Figure 11. Synchronized EM gradiometer receiver block diagram

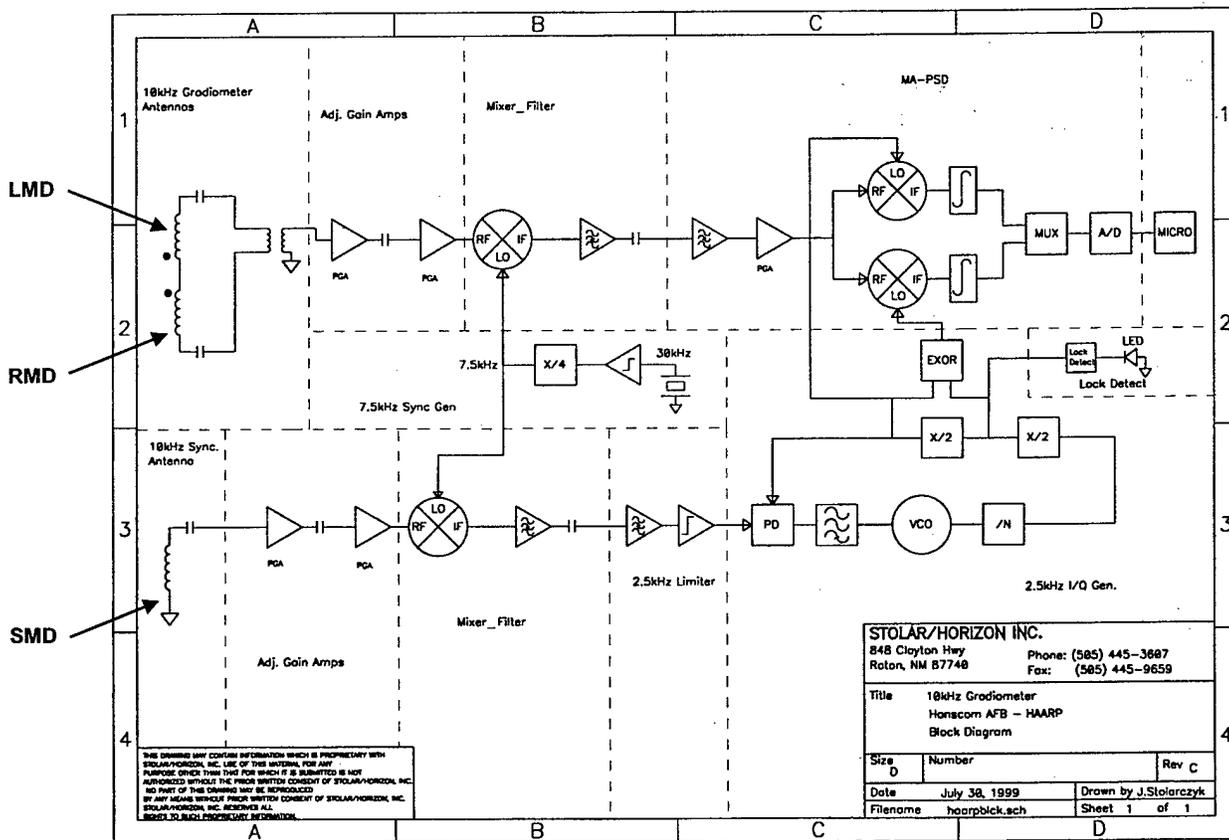The synchronized EM gradiometer receiver design has been partitioned into thirteen (13) circuit elements. The synchronizing magnetic dipole (SMD) antenna is a series tuned induction coil and followed by amplification greater than 138 dB (a signal path gain factor of 7.94 million). A single conversion design is required to prevent self-oscillations by providing some gain at the sync frequency (60 dB) and the remaining gain (78 dB) at the receiver intermediate frequency (IF). The EM wave magnetic field component threading the area of the induction coil, consisting of N number of turns, produces an electromotive force voltage (emf) that is given by

$$emf = -N \frac{d\phi}{dt} \qquad (8)$$

where ϕ = BA is the magnetic flux in Webers and B is the magnetic flux density in Tesla (Weber per square meter). A is the effective area of the magnetic dipole antenna in square meters.

For a sinusoidal magnetic flux, the emf voltage induced in the antenna is given by

$$emf = iN\omega (\mu_r A) B \qquad (9)$$

where N is the number of turns of the electrical conductor used in building the induction coil wound on the ferrite rod

and u_r is the relative permeability of the ferrite rod antenna.

The relative permeability for ferrite rods of different initial permeability and length-to-diameter ratio are shown in Figure 12.

Slug Permeability vs. Slug Length divided by Slug Diameter
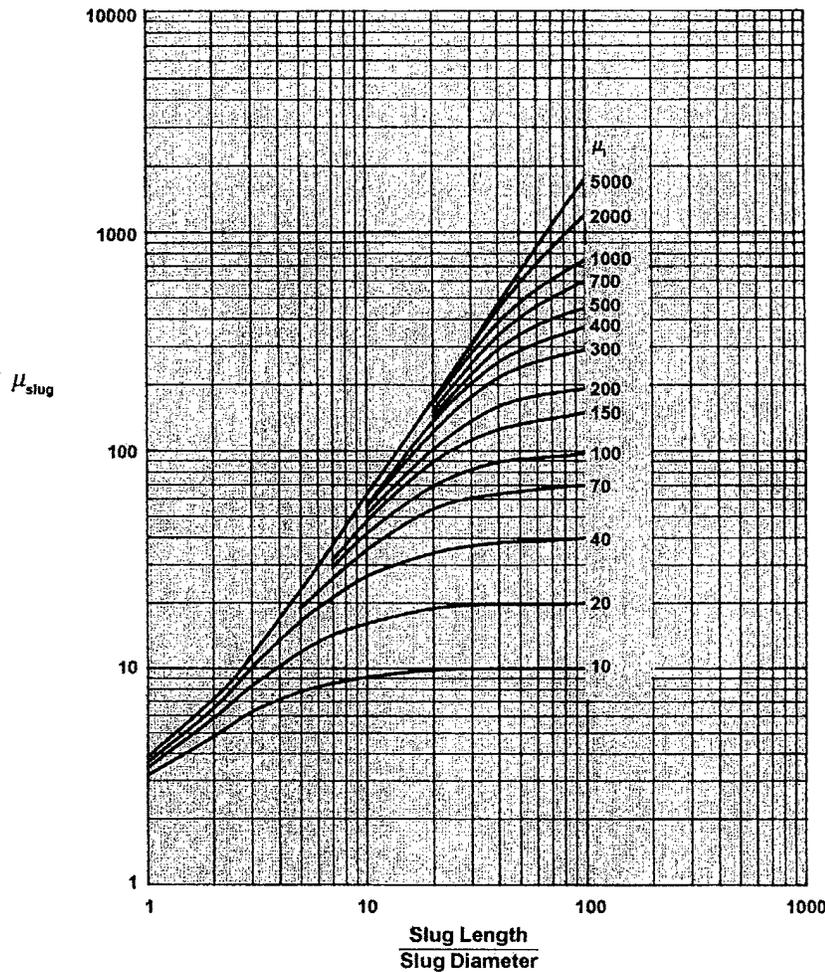
Figure 12. *Relative permeability versus rod length to diameter ratio*
(source: Fair-Rite Products Corp., Wallkill, NY)

A ferrite rod with an initial permeability of 5,000 and a length/diameter ratio of 12 achieves a relative permeability of 120. The induced emf increases with the first power of N and operating frequency ω, therefore, the modulation frequency used should be as high as possible to take advantage of ω in equation (9), but still low enough for the illuminating primary wave to encounter a low attenuation rate. The voltage also increases with the first power of effective area $(\mu_r A)$ and magnetic flux density (β) of the illuminating EM wave.

For a 1-inch diameter ferrite rod, the area is given by

$$A = \pi \left(0.0127\right)^2 = 5.07 \times 10^{-4} \text{ square meter.} \tag{10}$$

The HAARP 10-kHz transmitter modulation of the electrojet signal is expected to produce a picoTesla (10^{-12} Webers per square meter) signal causing the ferrite rod induction coil to produce a signal given by

$$\text{emf} = -i \left(850\right)\left(2\pi \times 10^4\right)\left(\left[120\right]5.07 \times 10^{-4}\right)\left(10^{-12}\right) \tag{11}$$

$$= -i \, 32\mu V \text{ per picoTesla.}$$

Figure 9 suggests that noise is expected to be 0.02 picoTesla in a 1-Hertz bandwidth. The S/N ratio would be

$$\text{SNR} = \frac{32 \times 10^{-12}}{.02 \times 32 \times 20^{-12}} = 50. \tag{12}$$

5. SYNCHRONIZATION CHANNEL

The primary EM wave illuminating the earth's surface is received by the series tuned sync magnetic dipole antenna (SMD). The emf signal (32 μV per picoTesla) is amplified by the programmable gain controlled amplifier (PGA) (60 dB of gain). The mixer-filter results in the frequency transposition of the HAARP signal to a 2.5-kHz intermediate frequency (IF) signal (additional gain of 78 dB). The IF signal is filtered and limited to form a square wave. The square wave signal is applied to the phase-locked loop (PLL) phase detector (PD). The PD and voltage-controlled oscillator (VCO) produce the in-phase (I) and quadrature (Q) sampling gate signals.

6. SYNCHRONIZED GRADIOMETER RECEIVER

The differential mode radiometer antenna (LMD and RMD) array produced the output signal (e_o) given by

$$e_o = emf_1 - emf_2. \tag{13}$$

The EM gradiometer array signal (e_o) is amplified by programmable gain control amplifier (PGA). The mixer-filter circuit results in the frequency transposition of the gradiometer signal to the 2.5-kHz intermediate frequency (IF) signal. The IF gradiometer signal is applied to the in-phase (I) and quadrature (Q) sampling gates.

The I and Q gate output signals are applied to separate integrators. The output of each integrator is applied to an analog-to-digital converter (A/D). After integration, the rectified signals are represented by

$$e_I = Ae_o \sin\theta \tag{14}$$

and

$$e_Q = Ae_o \cos\theta \tag{15}$$

where Ae_o is the magnitude of the amplified gradiometer signal and A is the total signal path gain, and

     θ is the phase of the gradiometer array signal and the signal path phase shift.

The squared magnitude of these signals is given by

$$M = \sqrt{e_I^2 + e_Q^2} = Ae_o \tag{16}$$

and the phase by

$$\theta = \tan^{-1} e_I / e_Q. \tag{17}$$

In overt detection and imaging, a compact horizontal magnetic dipole can be deployed along with the synchronized EM gradiometer receiver as a surface-based system. When access is denied, the HAARP transmitter and other standoff sources of EM wave fields propagating in the earth-ionosphere waveguide will illuminate the surface overlying the underground facility.

The HAARP Ionospheric Research Observatory is a new facility currently under development near Gakona, Alaska. The present HAARP HR transmitting system includes a phased-array antenna, consisting of 48 elements, with crossed-dipole antennas driven individually by 10-kW transmitters, resulting in a maximum radiated power of 960 kW.

Fundamentally, the earth-ionosphere waveguide provides a means of propagating EM fields to the clandestine tunnel and UGC site for site illumination purposes. As illustrated in Figure 13, the waveguide supports the quasi TEM mode.
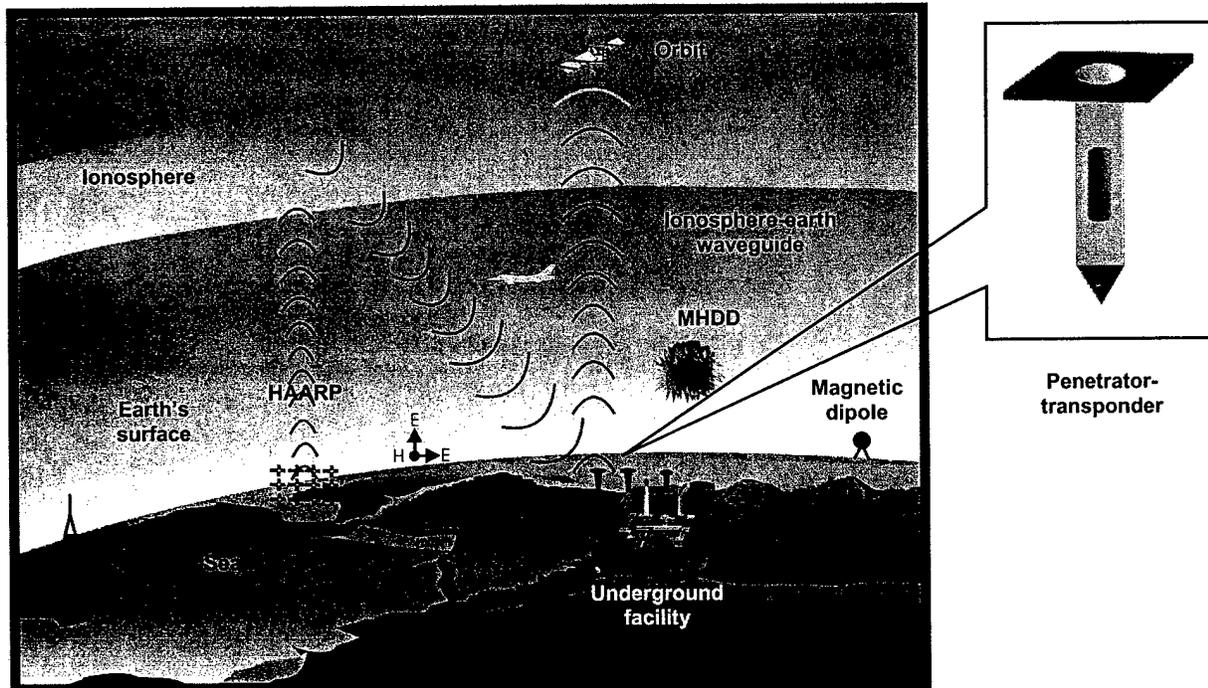

Figure 13. Electromagnetic wave sources

Measurement of the horizontal E and H components is used in determining the electrical conductivity of the soil overlying the UGC. On the far left side of Figure 13, an indigenous transmitter is illustrated as an opportunistic source of quasi TEM signals. The Navy very-low-frequency transmitter, located in Washington state (output power of 2.3×10^5 watts), is an example of a potential opportunity source. The quasi TEM wave vertical electric field has been analytically determined to be 2.2 mV/m at the NTS. The experimental value was found to be 2.6 mV/m. Aircraft equipped with horizontal magnetic dipole antennas are used in geophysical exploration. Very strong EM signals can be created by induction coils designed into chemical explosives—magnetohydrodynamic devices (MHDD). An MHDD was developed into a borehole radar logging tool for the oil/gas industry. The industry did not accept the radar design because of possible damage to multimillion-dollar wells. We speculate that MHDD detonating over a UGC just prior to and during attack can be made into an effective MHDD EM source.

The synchronized EM gradiometer receiver technology can be reconfigured into a penetrator-transponder (PT). PT could become an important tool for acquiring UGC response data prior to and during an attack. The PT could include an S-band transmitter for communicating collected data to overhead vehicles. The PT could be deployed along survey line(s) crossing the heading of the adit and the suspect UGC target. Several PTs could form a gradiometer array. Each PT can be equipped with microelectromechanical system (MEMS) to monitor seismic activity. The seismic data would be processed in microseismic algorithms developed for the mining industry. These data can determine distance to the underground roadway, and map the orientation of entries in the UGC. A built-in global positioning system (GPS) receiver will provide physical location data.

The transmitter (TX) simulating the HAARP electrojet signal in field data acquisition has power output from 960 kW presently to potentially 3.6 MW on completion.

7. FIELD DATA ACQUISITION INSTRUMENTATION

The horizontal magnetic dipole bistatic scan method causes the sync EM gradiometer receiver (background) and companion transmitter (foreground) to move in unison across the survey area. The transmitter horizontal magnetic dipole antenna is located on the bisector line between the two EM gradiometer horizontal magnetic dipole antennas (Figure 14).
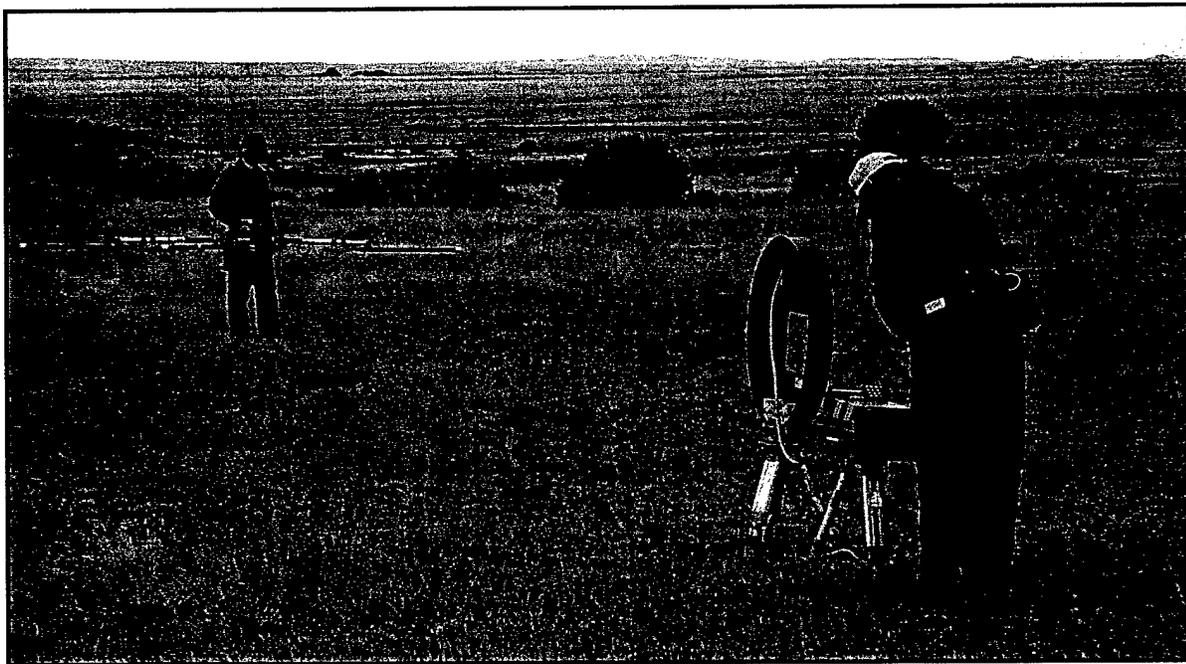

Figure 14. Bistatic EM gradiometer instrumentation

The companion transmitter (TX) used for field testing generates the 10-kHz primary EM wave. The TX is a portable antenna supported on a tripod. The best radiation coupling occurs when the loop plane points parallel to the trend of the intended target.

In the field, the transmitter is powered on and switched into continuous transmit mode while the operator moves from station to station. The operator's responsibilities include TX positioning and monitoring of loop current.

We evaluated two EM gradiometer instrumentation system configurations: fixed transmitter (fixed offset) and bistatic. For the fixed offset transmitter configuration, the transmitter was set up at a specific location and then the gradiometer moved along the survey baseline. For the fixed offset and bistatic configurations, the EM gradiometer receiver is moved along a survey baseline and measurements made at constant intervals.

8. FIXED DATA COLLECTION SITES

EM gradiometer field trials were conducted at four different test sites:

♦ NRA Whittington Center, near Raton, New Mexico

♦ Otay Mesa drug smuggling tunnel, near San Diego, California

♦ Silver Fox Mine, near Fairbanks, Alaska

♦ Permafrost Tunnel, near Fairbanks, Alaska

9. NRA WHITTINGTON CENTER BURIED CONDUCTOR SURVEY RESULTS

During the field testing of the EM gradiometer receiver systems, three different types of conductor configurations were included in the test plan. A very shallow phone line, a deeply buried 18-gauge wire, and an overhead power line were used to simulate a buried tunnel. The phone line survey included fixed offset and bistatic surveys with baseline separations of 25, 50, 75, and 100 feet. The telephone line was buried about 1 foot deep and was several thousand feet in length.

The buried 18-gauge AWG wire survey included fixed offset and bistatic surveys with baseline separations of 50, 100, 200, and 300 feet. The line was buried about 4 feet deep and was just under a thousand feet in length. The wire was laid into a 6-inch wide PVC water pipe trench before being re-buried and then grounded on each end using 4-foot ground rods.

10. FIXED OFFSET SURVEY METHOD

During the fixed offset survey mode, the TX antenna is placed at a fixed distance from the buried conductor, and the plane of the loop antenna is positioned parallel to the heading of the conductor. The EM gradiometer receiver then measures the gradient of the scattered wave at predetermined intervals on a baseline perpendicular to the buried conductor. The survey configuration is diagrammed in Figure 15.
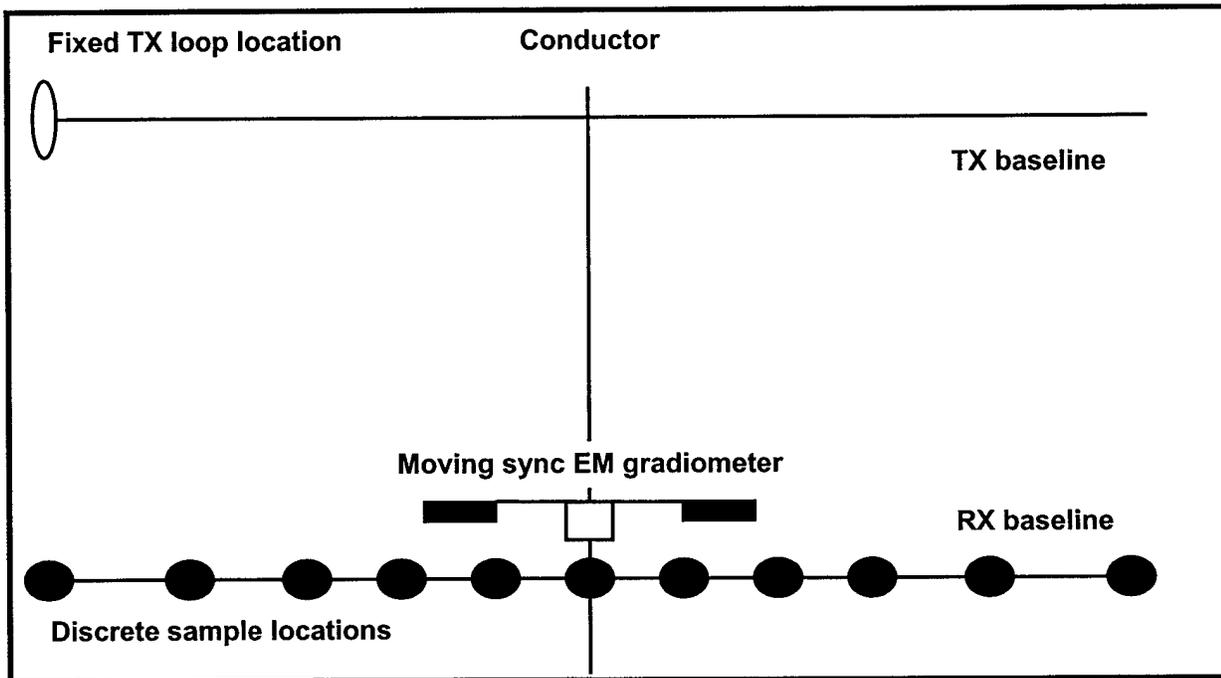
Figure 15. Scan with offset transmission

Once the EM gradiometer receiver baseline is surveyed for a discrete sample location, the TX is positioned at a fixed distance from the conductor and the survey line is surveyed for each TX fixed position. The resulting data set contains sync EM gradiometer receiver survey profiles over the conductor for six different TX offset distances: 50, 40, 30, 20, 10, and 0 feet from the conductor's surface projection line.

The acquired data are graphically constructed in Figure 16. These data show the effect of the conductor heading not being perpendicular to the survey lines.
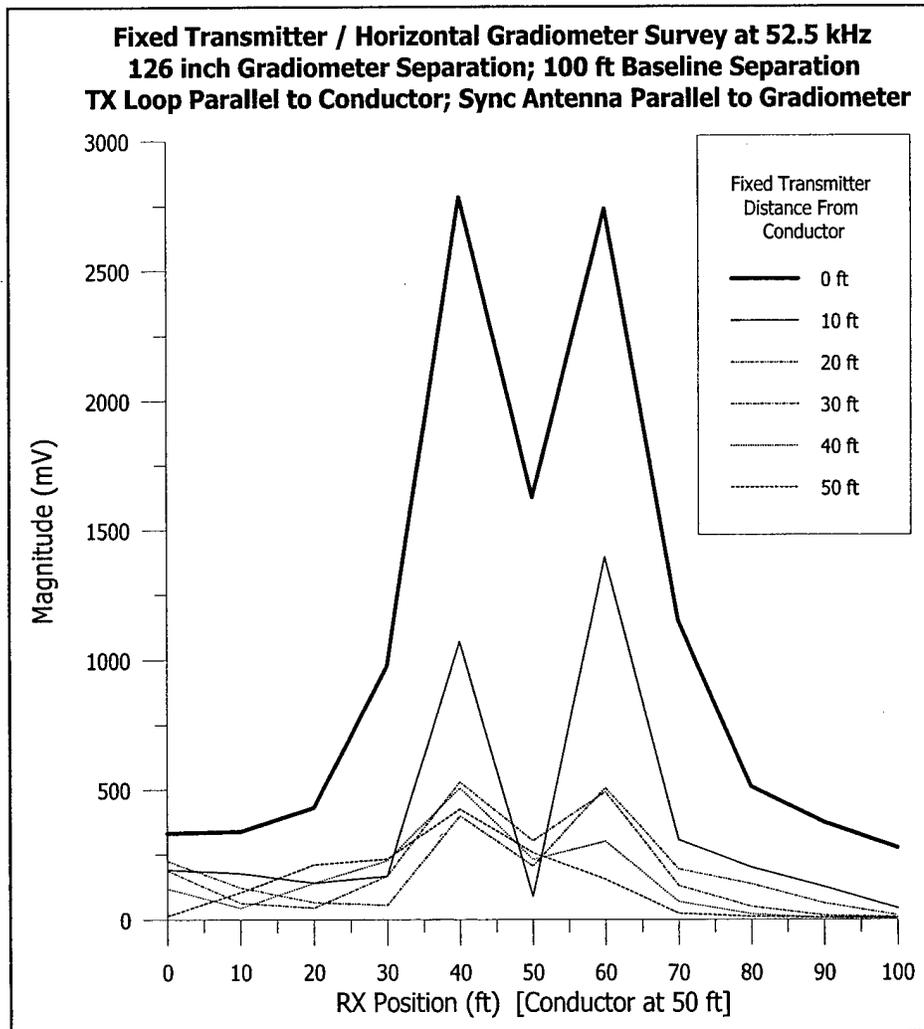
Figure 16. Measured data for fixed offset configuration

These data suggest that the peak response will not be symmetrical in the event that the buried conductor is not at a right angle to the traverse.

There is a perceptible anomaly for each fixed TX position with equal locations for the two peaks and central minimum. Unfortunately, the sampling interval was too coarse (10 feet) to accurately determine the buried depth from the anomaly profile because the location of the magnitude peaks falls between measurement locations. A finer sampling interval of 6 to 12 inches over the conductor would have allowed a determination of burial depth by measuring the distance between the maximum peaks.

11. BISTATIC SURVEY METHOD

During the bistatic survey the TX antenna is kept positioned parallel to the conductor and at the same location along its baseline as the center line of the LMD and RMD gradiometer antennas. The sync EM gradiometer receiver then measures the gradient of the scattered wave at predetermined locations along a baseline. The bistatic survey configuration is diagrammed in Figure 17.
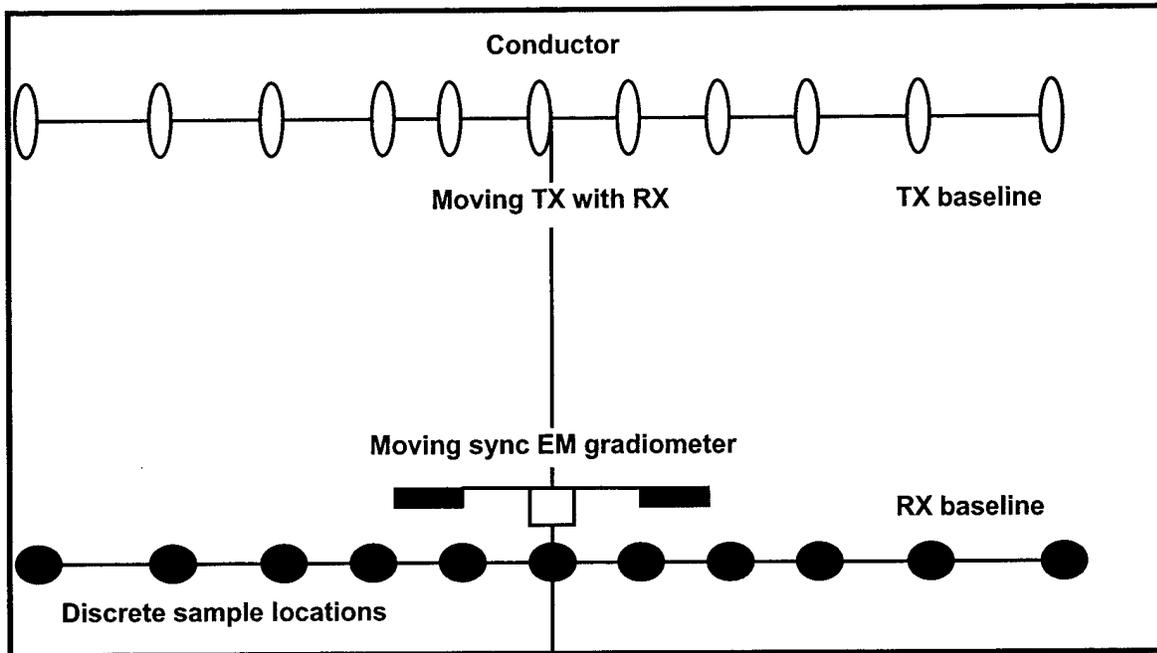
Figure 17. Bistatic survey method

The bistatic survey data at a 100-foot baseline separation are shown in Figure 18 for both the vertical and horizontal sync EM gradiometer antenna positions. The profiles are relatively the same for both antenna positions. The sampling interval of 2 feet shows a maximum peak separation of 4 feet. This separation is equal to the conductor's depth of burial.
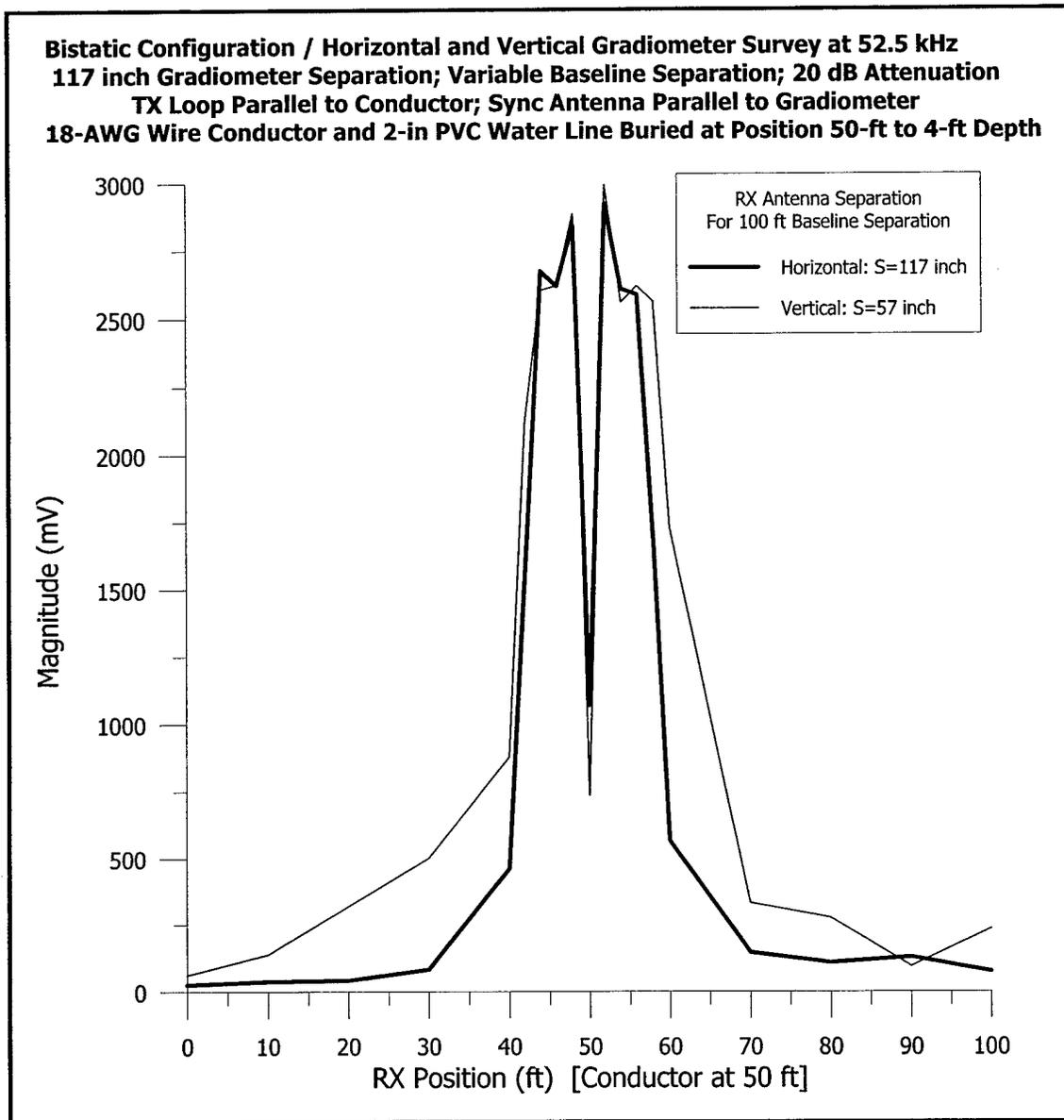
Figure 18. *Measured data for bistatic scan configuration*

The peak-to-peak separation distance is approximately 4 feet, the burial depth. The vertical

gradiometer position simulates the response expected from a penetration array. The overhead

power line survey included fixed offset surveys with baseline separations of 100 and 200 feet, as

well as a continuously recording walk survey during which the sync EM gradiometer operator

paced the baseline while continuously measuring data. The power line consisted of a single line

25 feet off the ground, and a second line directly above it at 29 feet above the surface. The fixed

offset survey data were acquired with a 200-foot baseline separation distance. There is a

perceptible anomaly for each TX position with equal locations for the two peaks and central

trough when the TX was as close as 30 feet from the conductor's surface projection. The

sampling interval of 5 feet shows a maximum peak separation of nearly 30 feet (see Figure 19).

This separation is approximately equal to the conductor's height above the ground.

Monostatic Fixed Transmitter / Horizontal Gradiometer Survey at 52.5 kHz
117 inch Gradiometer Separation; 200 ft Baseline Separation; 10 dB Attenuation
TX Loop Parallel to Conductor; Sync Antenna Parallel to Gradiometer
2 Overhead Power Line Conductors Above Position 50-ft at Heights 25 and 29 ft.

Continuous Measurement Walk (50 average)

Fixed Transmitter Location:
Discrete 5-ft Measurements (200 average)

Tx at 0 ft : 50 ft from conductor

Tx at 10 ft : 40 ft from conductor

Tx at 20 ft : 30 ft from conductor

Tx at 30 ft : 20 ft from conductor

Tx at 50 ft : Directly over Conductor

Figure 19. Measured data for fixed offset configuration

A photograph of the Otay Mesa drug smuggling tunnel site is shown in Figure 20.

Shaft and hoist in this building

Site of suspect tunnel

Border and alien fence

***Figure 20.** Aerial photograph of the Otay Mesa drug smuggling tunnel site*

Figure 21 illustrates the sync EM gradiometer receiver traverse lines along with measured data.

The tunnel was developed from the Mexican side of the US border toward an unfinished warehouse (a tomato canning factory), now a Federal building at Otay Mesa. The tunnel
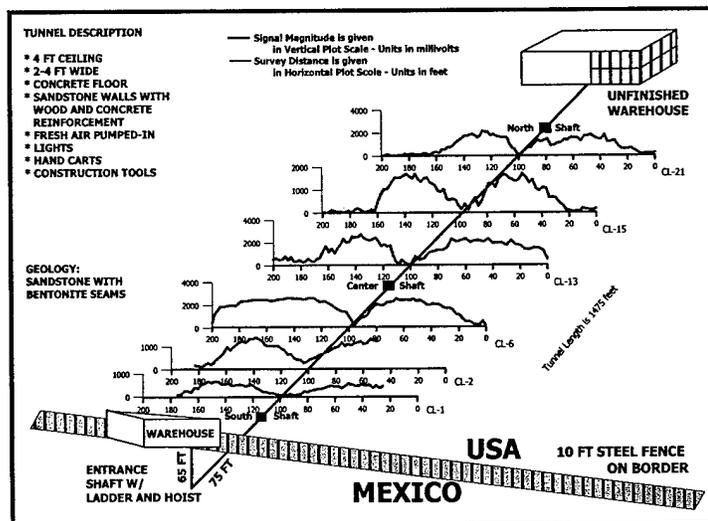
***Figure 21.** Otay Mesa drug smuggling tunnel with sync EM gradiometer measured data*

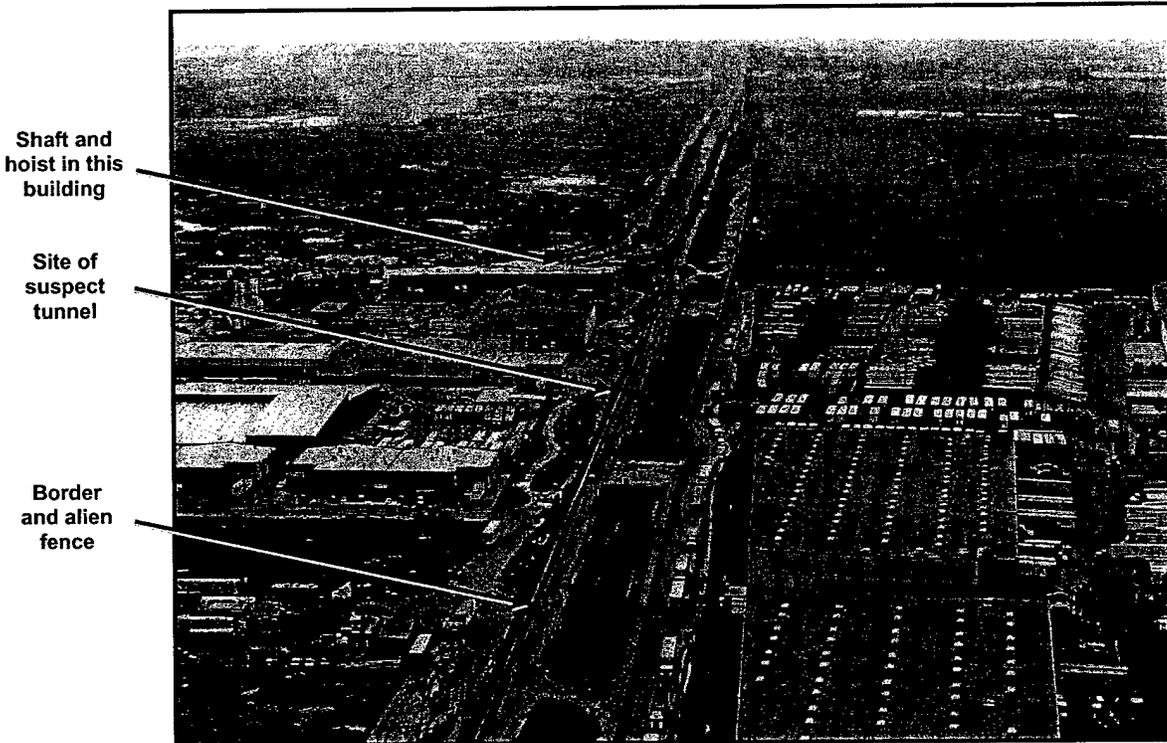miners are incarcerated in the San Diego area. The canning factory was under construction at the time of discovery in 1991 (see Figure 22).
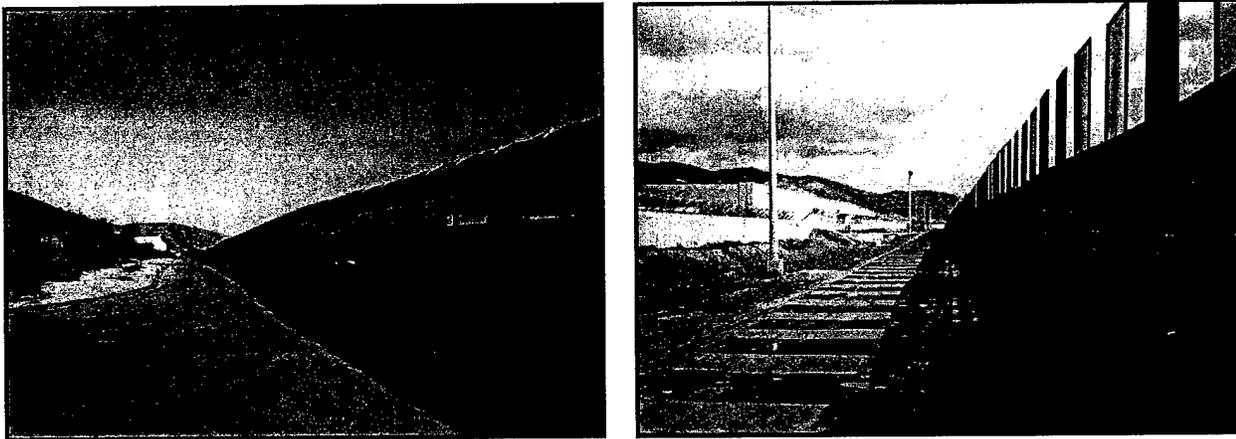
a) North side of alien fence   b) North side of border fence

Figure 22. Photograph of tunnel crossing site

Deception was practiced at the entrance within the warehouse. A shower with a large drain cover disguised the tunnel entrance. The cross section of the tunnel is illustrated in Figure 23.

Figure 23. Cross section of the Otay Mesa tunnel

The tunnel was developed in ash fall tuff. Ground control near the border consists of timber framing. On the northern end of the tunnel, ground control was intensified to include reinforced concrete. The photograph (Figure 24) shows the interior of the tunnel near the border fence.
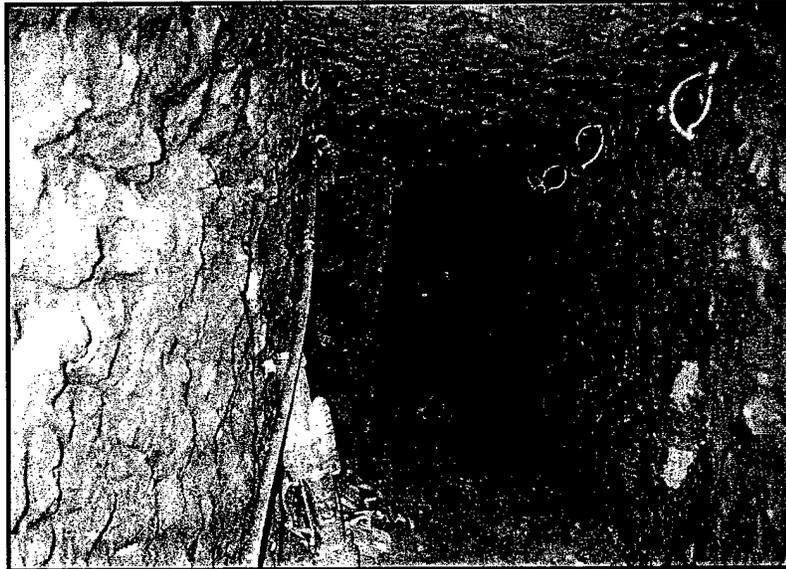
Figure 24. Northern direction of a photograph of the interior of the tunnel

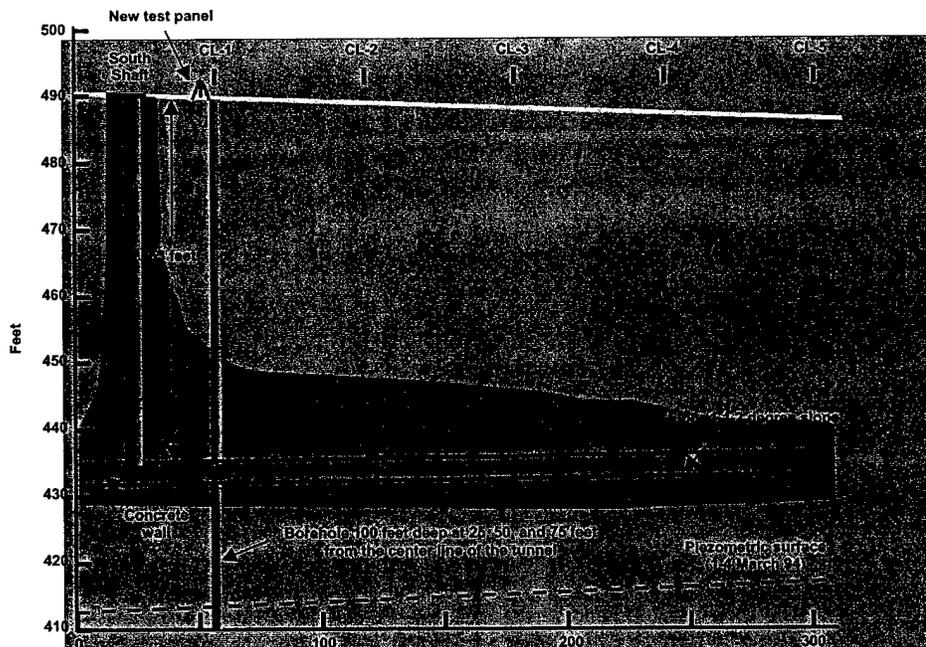The three-phase electric power cable appears on the left-hand wall. An electric light bulb is also seen on the left-hand wall. Wire-reinforced ventilation tubing was installed on the brackets on the right side of the wall. The ventilation tubing was removed some time after discovery.

The EM gradiometer data were acquired during traverses over the center line of the tunnel. The data were acquired at walking speed. Because the S/N ratio of the sync EM gradiometer receiver response is very high, data processing is not needed. The tunnel response was immediately displayed at the field site. The data are shown in graphical form in the following illustration (Figure 25). The depth is determined from the peak-to-peak separation as illustrated in Figure 25.

Measured data

Otay Mesa Known Tunnel REMGA Traverse - January 28, 1999
126-inch Separation Horizontal RX Gradiometer over 200 ft Baseline at CL-15
Fixed TX on CL-17 Marker; Baseline Separation is 100 ft
Tunnel Centerline at 100 Ft Baseline Position; Continuous Sampling
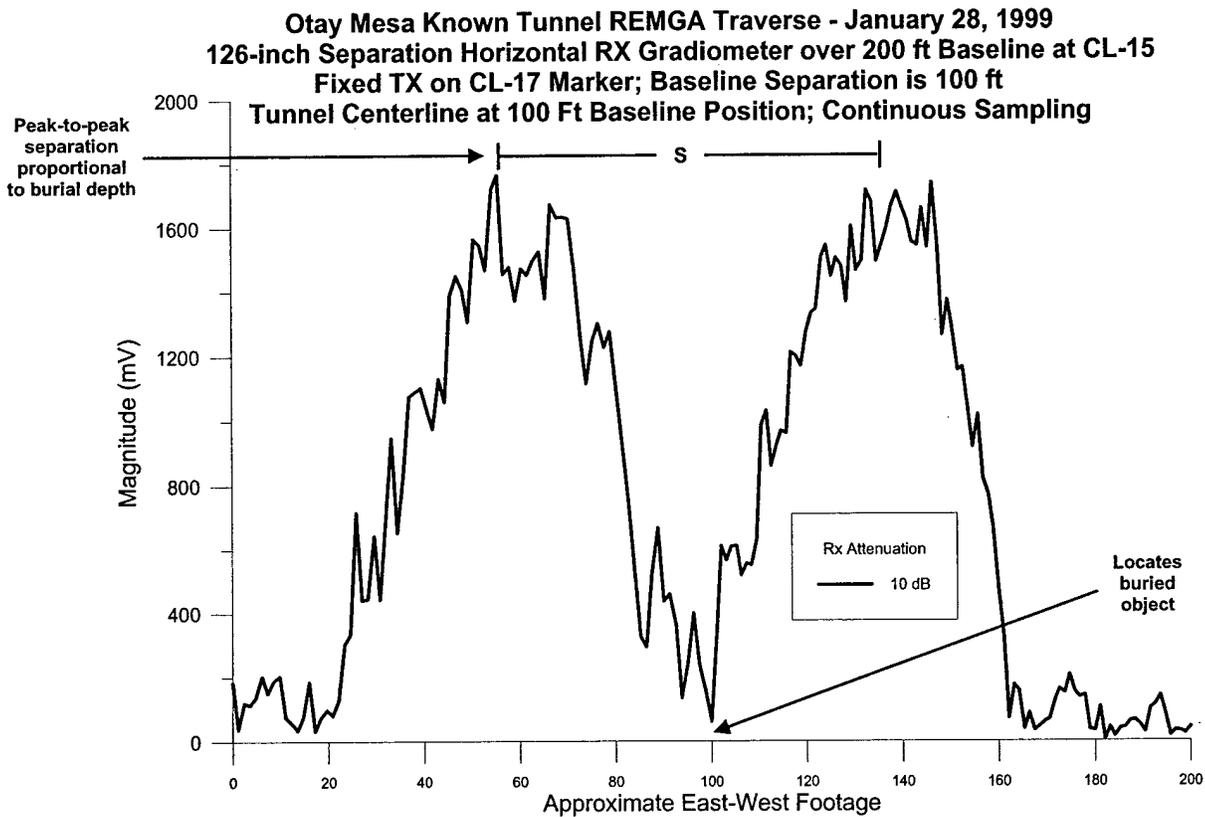
Figure 25. EM gradiometer acquired data

Robert Kelly [16] has developed an approximation formula for determining depth of burial as

$$\text{depth} \approx S \times \frac{1}{2}\sqrt{3} . \tag{18}$$

The formula assumes plane wave propagation through the earth-air interface. The formula

needs to be modified for the cylindrically spreading secondary wave. The following table shows

the depth estimates along the tunnel center lines (CL) as illustrated in Figure 21. The depth

determined from the acquired data is shown in the table.

RX Traverse Position (CL #)	Description of CL# Locations Relative to Surface Structures (Shafts or Fences) Traverse Baseline Length	Tunnel Depth from Geotech Maps (ft)	Tunnel Depth Estimate Based on REMGA Profile Peak to Trough Separation (ft)		% Depth Estimate Variation
CL-21	250 ft south of North Shaft	max 40	Left Peak – Center	43	
(Tx @ CL-24)	200 ft baseline perpendicular to center line	min 34	Right Peak – Center	45	18.9
CL-15	150 ft north of Center Shaft	max 41	L	40	
(Tx @ CL-24)	200 ft baseline perpendicular to center ine	min 37	R	48	12.8
CL-13	50 ft north of Center Shaft	max 42	L	44	
(Tx @ CL-24)	200 ft baseline perpendicular to center line	min 38	R	50	17.5
CL-6	250 ft south of Center Shaft	max 47	L	49	
(Tx @ CL-24)	200 ft baseline perpendicular to center line	min 43	R	49	8.9
CL-2	125 ft north of South Shaft – 20 ft north of North Fence	max 51	L	64	
(Tx @ CL-3)	135 ft baseline perpendicular to CL – east end near canal	min 47	R	64	30.6
CL-1	75 ft north of South Shaft – 35 ft south of North Fence	max 52	L	52	
(Tx @ CL-3)	150 ft baseline perpendicular to center line near Borings	min 48	R	50	2.0
CL-SSR	15 ft south of South Shaft – 10 ft north of South Fence	max 53	L	50	
(Tx @ CL-3)	150 ft baseline perpendicular to center line on road	min 49	R	52	0.0

12. SUSPECT TUNNEL

The US Border Patrol has collected information from informants that passageways have been developed in the Otay Mesa border crossing area. The local region has many miles of built-up warehouses and commercial facilities on both sides of the border. A sync EM gradiometer scan was run between the alien and Mexican border fence resulting in the anomalous gradiometer response shown in Figure 26.

From these data, the location of the center line can not be accurately determined; however, the approximate depth of the suspect tunnel ranges between 50 and 60 feet. Drilling has not intercepted this tunnel; however, the cutting did provide evidence of a cement layer. The site is

still being investigated and the drug smuggling cartel may have used backfilling as deception at this site.
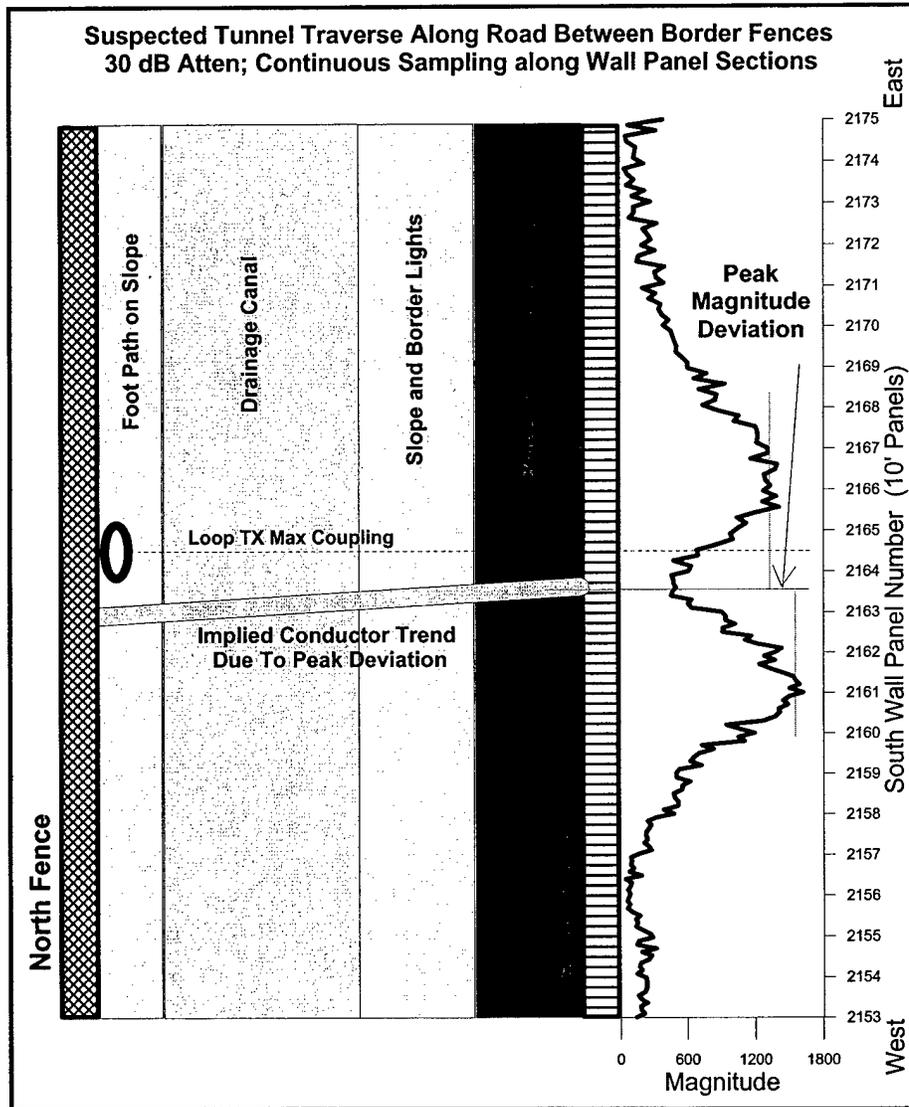

Figure 26. *Response of the suspect Otay Mesa tunnel*

The US Border Patrol is preparing a drilling plan that will enable borehole-to-borehole radiowave tomography of the suspect tunnel threat zone along the fence.

13. SILVER FOX MINE

The Silver Fox Mine is a research facility owned and operated by the University of Alaska at Fairbanks. Originally a privately owned gold, silver, and lead mine, the Silver Fox is currently used by the University of Alaska at Fairbanks to conduct research and teaching programs by its Mining and Geological Engineering Department. The mine is at a site 17 miles north of Fairbanks, Alaska. Figure 27 is a plan view drawing of the Silver Fox Mine.

The main adit contains electrical cable for power, steel pipe, and steel narrow-gauge track rail. The mine's geology is predominantly schist and the soil over-burden is relatively shallow. The adit of the Silver Fox Mine is shown in Figure 28.
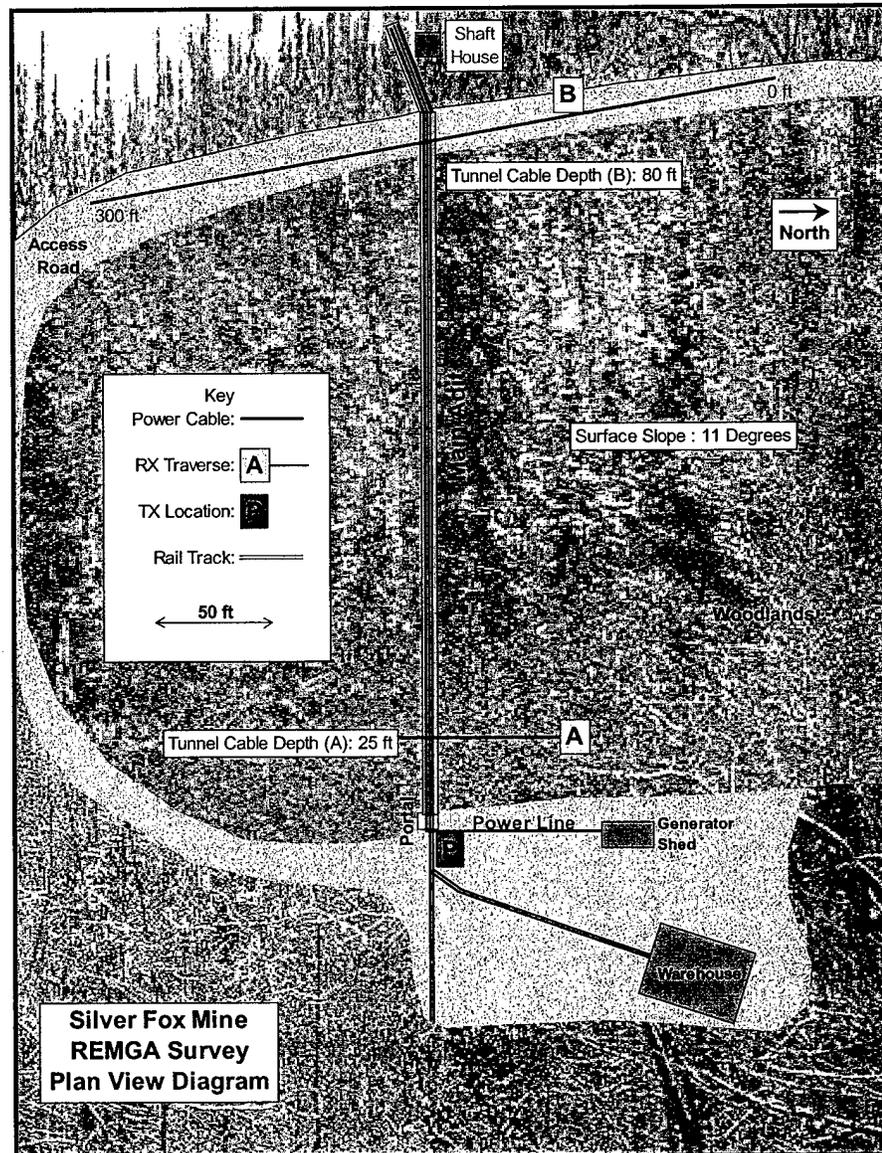

Figure 27. Plan view drawing of Silver Fox Mine

Figure 28. Photograph of the Silver Fox Mine adit

The survey technique employed at the Silver Fox Mine was the Fixed Transmitter Survey Method. The transmitter was coupled onto the tunnel's main power lines at the portal. The loop was always kept parallel to its nearest conductor cable. This ensured maximum coupling and induced current.

The sync EM gradiometer receiver surveyed along two (2) different traverse lines from north of the adit's center line to south of the center line. Measurements were discretely sampled over these traverses at 5-foot intervals. The survey traverse locations where placed so that the EM gradiometer response would cross the adit at right angles, maximizing the expected anomalies. The locations of the traverses and conductors with respect to the mine's main adit are shown along with the graphical data in Figures 29 and 30.
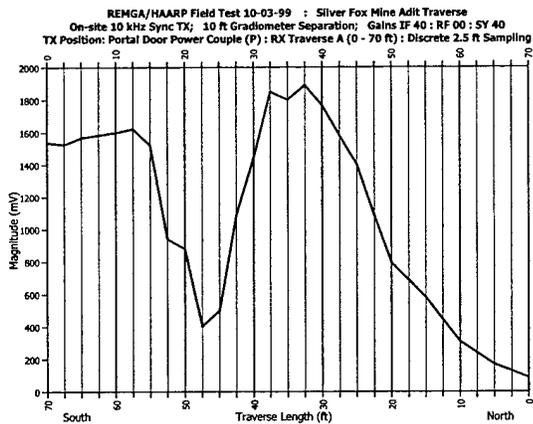
Figure 29. *EM gradiometer response versus distance along the A survey line*
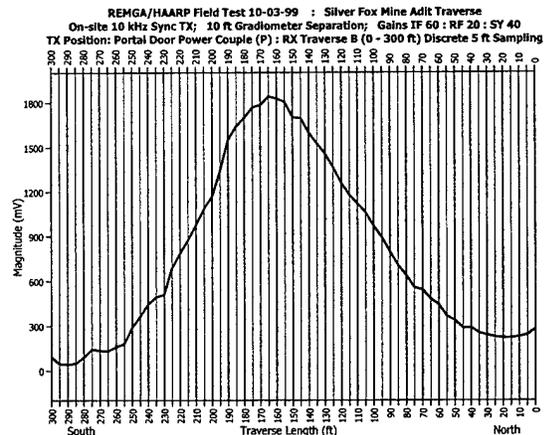
Figure 30. *Summation mode EM gradiometer response versus distance along the B survey line*

The measurements recorded over the A and B traverses were plotted against position to show the locations at which the sync EM gradiometer Silver Fox Tunnel response peaked and nulled. In the Horizontal Gradient Mode, detection can be characterized by a pair of increased magnitude peaks centered by a trough in the profile. Traverse A exhibits a trough indicating the relative position of the tunnel's center line on the surface. During the B traverse surveys, the EM gradiometer receiver antenna array was operated in a Summation Mode. The receiver antennas were coupled to operate as a single dipole antenna measuring the total horizontal magnetic field component. In this mode, a peak occurs over the tunnel.

14. COLD REGIONS RESEARCH AND ENGINEERING LABORATORY (CRREL) TUNNEL

Field testing of the sync EM gradiometer instrumentation was conducted at the Cold Regions Research and Engineering Laboratory (CRREL) Permafrost Tunnel Site on October 2 and 4, 1999. A 10-kHz transmitter was placed near the tunnel adit.

The Permafrost Tunnel, located 10 miles north of Fairbanks, Alaska, is maintained by the US Army Corps of Engineers (Figure 31).

The tunnel is situated near the valley floor of Goldstream Creek and was excavated entirely within perennially frozen silt and gravel. The site is immediately adjacent to an area where dredge mining methods were used for placer gold mining during the first half of the century. Construction of the tunnel began in the 1960s using an Alkirk™ continuous-cycle mining machine. The facility is currently used as an active underground laboratory for a wide variety of research projects, paleoclimatic and sedimentological analyses of the Permafrost environment, geophysical analyses of Permafrost features, and geophysical application for tunnel and void delineation. A refrigeration system maintains the frozen status year round.
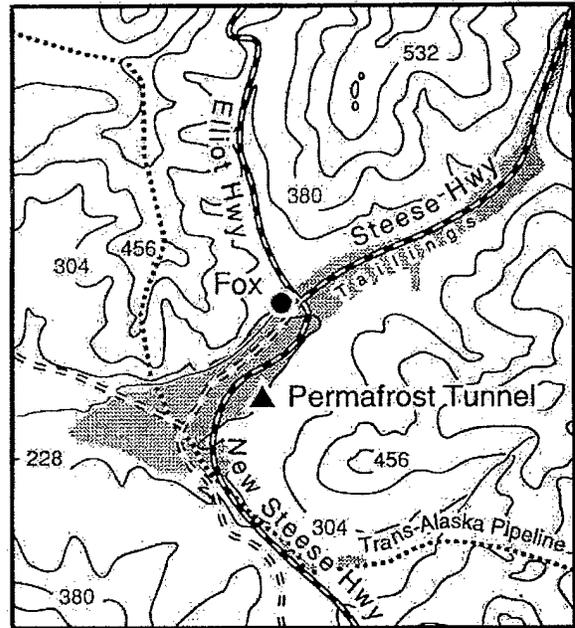
Figure 31. Location of the CRREL Permafrost tunnel

The tunnel's geology is predominantly fine-grain silt laden with organic remains and ice. The

Permafrost stratigraphy includes a diverse assemblage of animal fossils and plant remains.

Figure 32 is a photograph of the tunnel wall.

Figure 32. Photograph of the tunnel wall showing a Plains bison jawbone

Exposed in the tunnel walls are numerous types of ground ice, including ice wedges, ponds,

lenses, and pore fillings. Figure 33 is a plan view diagram of the CRREL tunnel showing the

location of all relevant conductors and traverse lines.

Figure 33. *Plan view diagram illustrating the CRREL tunnel*

Measurements were conducted over the B, C, D, E, and F traverses.

Figure 34 shows the location of electrical conductors within the tunnel.

The survey technique employed at the CRREL Permafrost tunnel was the Fixed Transmitter Survey Method. This method involved using the local transmitter to couple RF-frequency energy onto the tunnel's main power lines at and around the tunnel's entry portal for maximum coupling to the conductors in the tunnel. Figure 35 shows the positioning of the local 10-kHz transmitting loop antenna into the tunnel's power lines. The loop was located at the portal door and nearest to the conductor cable. This ensured maximum coupling and induced current. Also noted on the plan view drawing is the location of a surface power conductor.

The EM gradiometer receiver was then moved along five traverse lines from 100 feet east of the tunnel center line to 100 or 200 feet west of the center line. Measurements were discretely sampled over these traverses at 5-foot intervals. The traverse locations where placed so that the EM gradiometer receiver would cross the tunnel at right angles,

Figure 34. *Photograph of the inside of the Permafrost tunnel*
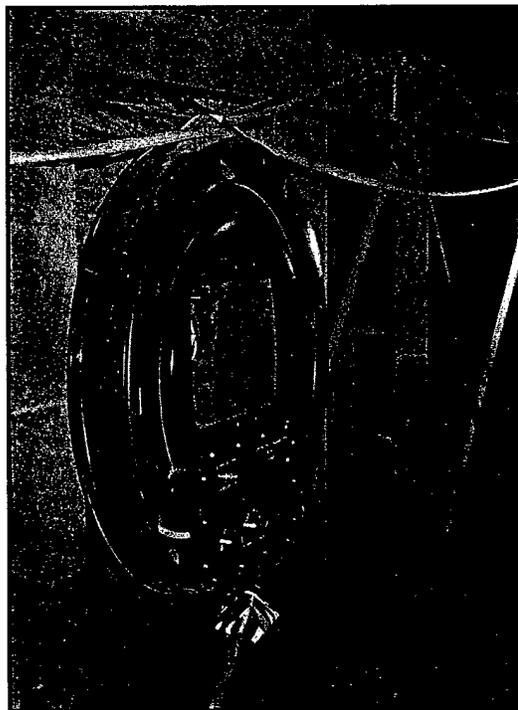
Figure 35. *Loop antenna coupling to power cables*

maximizing the expected anomalies. Several traverses crossed multiple conductors since there was an additional tunnel extension, the Winze Tunnel, as well as surface conductors. These additional conductors create complex anomalies.

15. ANALYSIS OF ACQUIRED DATA

The acquired data are graphically presented as the magnitude of the gradiometer response versus distance along survey lines shown in plan view of the survey area. The location of the surface power conductor, as shown in Figure 33, exits the portal and connects to the shaft house. An exposed section of the cable is shown in Figure 36.
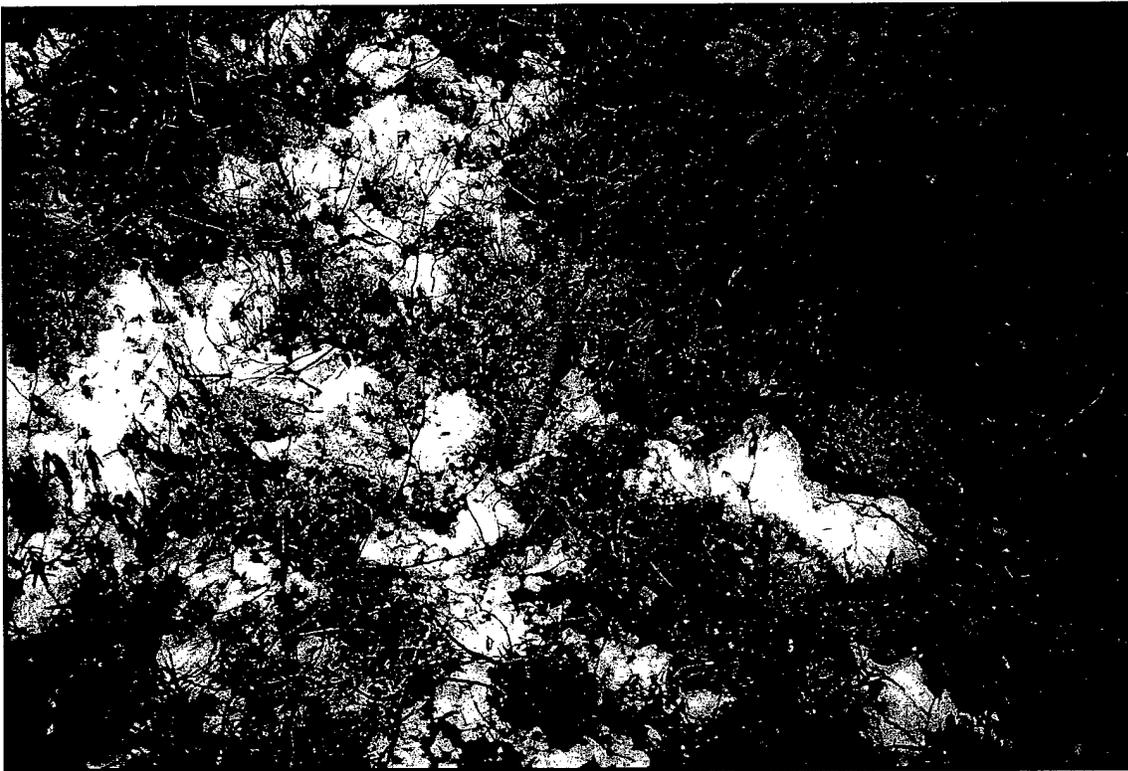
Figure 36. Photograph of the surface cable between the portal and shaft house

The acquired data sets are strongly influenced by the surface cable response. These data sets are shown in the following graphical figures.

15.1 B Traverse

REMGA/HAARP Field Test 10-02-99 : CRREL Permafrost Tunnel Traverse
On-site 10 kHz Sync TX; 10 ft Gradiometer Separation; Gain IF60:RF20:SY40
TX Position: Portal Door Power Couple (P) : RX Traverse B (0 - 200 ft) : Surface Conductor at 110 ft
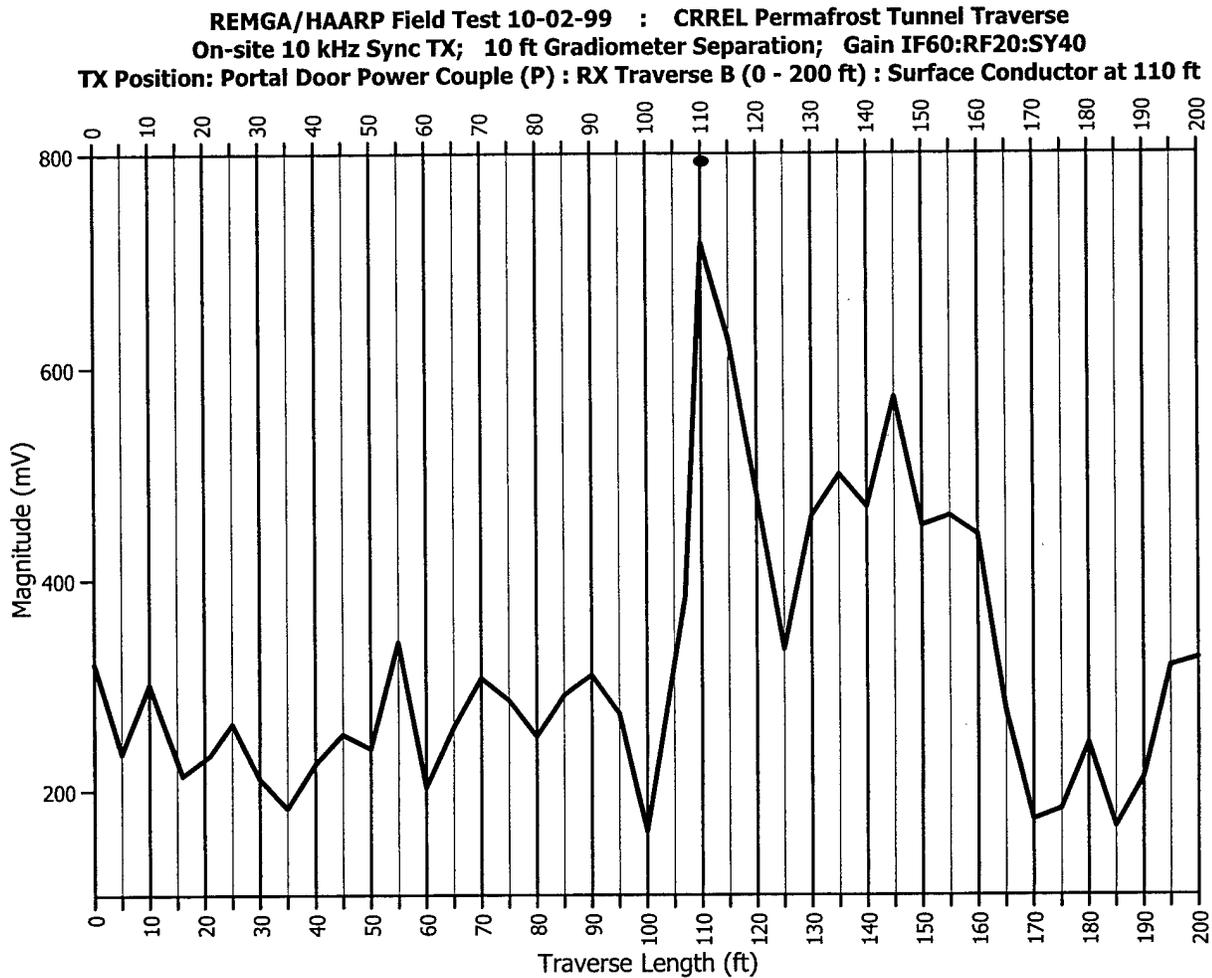
Figure 37. B traverse – EM gradiometer receiver response versus traverse distance in feet

The deep minimum at 100 feet occurs directly over the tunnel center line, however, the

surface cable response at 110 feet causes an even greater response. The EM gradiometer data

measured over the C traverse are graphically presented in Figure 38.

15.2 C Traverse

REMGA/HAARP Field Test 10-02-99 : CRREL Permafrost Tunnel Traverse
On-site 10 kHz Sync TX; 10 ft Gradiometer Separation; Gain IF60:RF20:SY40
TX Position: Portal Door Power Couple (P) : RX Traverse C (10 - 300 ft) : Surface Conductor at 115 ft
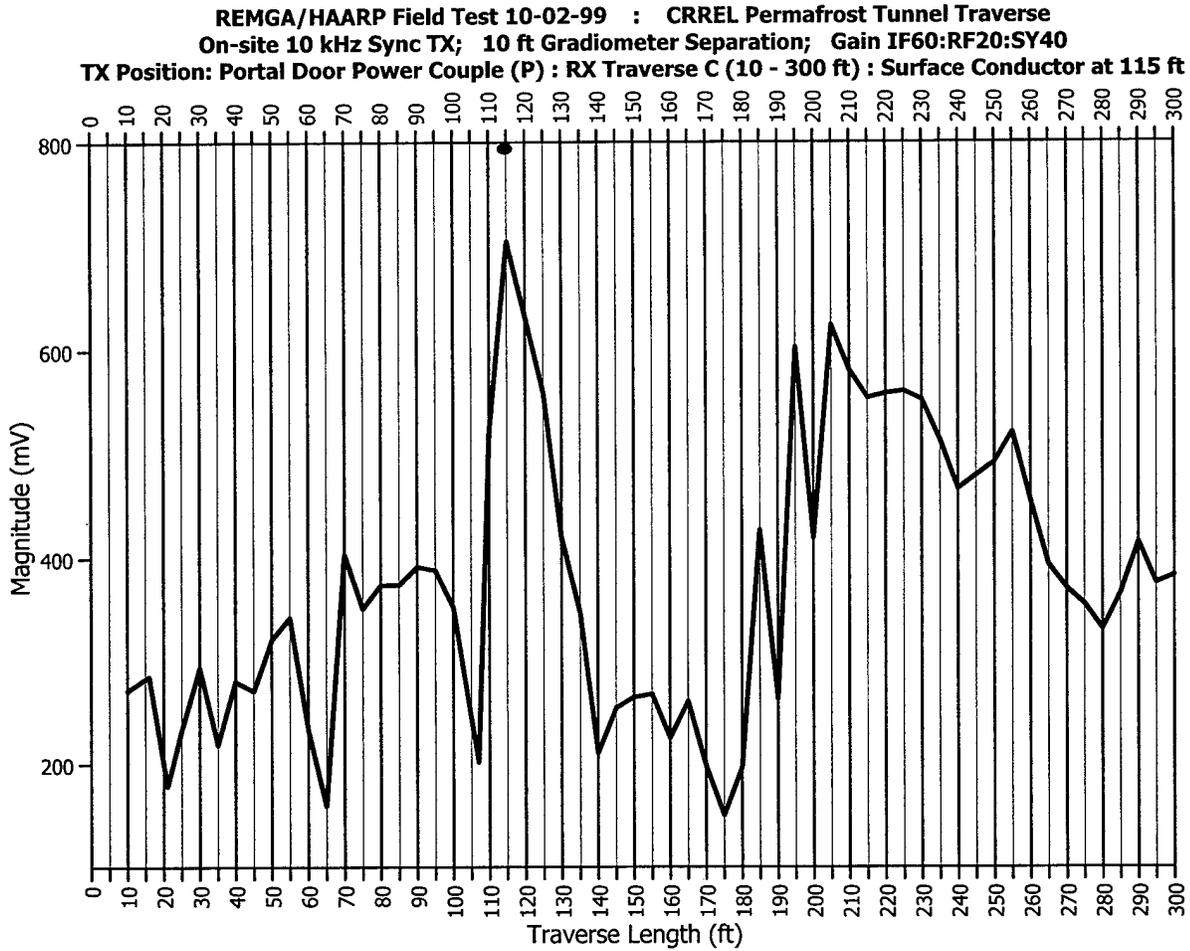
Figure 38. C traverse – EM gradiometer response versus traverse distance in feet

The cable response predominates over the center line of the tunnel. The deep minimum at 170 feet occurs over Winze Tunnel center line.

15.3 F Traverse

REMGA/HAARP Field Test 10-02-99 : CRREL Permafrost Tunnel Traverse
On-site 10 kHz Sync TX; 10 ft Gradiometer Separation; Gain IF60:RF20:SY40
TX Position: Portal Door Power Couple (P) : RX Traverse F (40 - 330 ft) : Surface Conductor at 115 ft
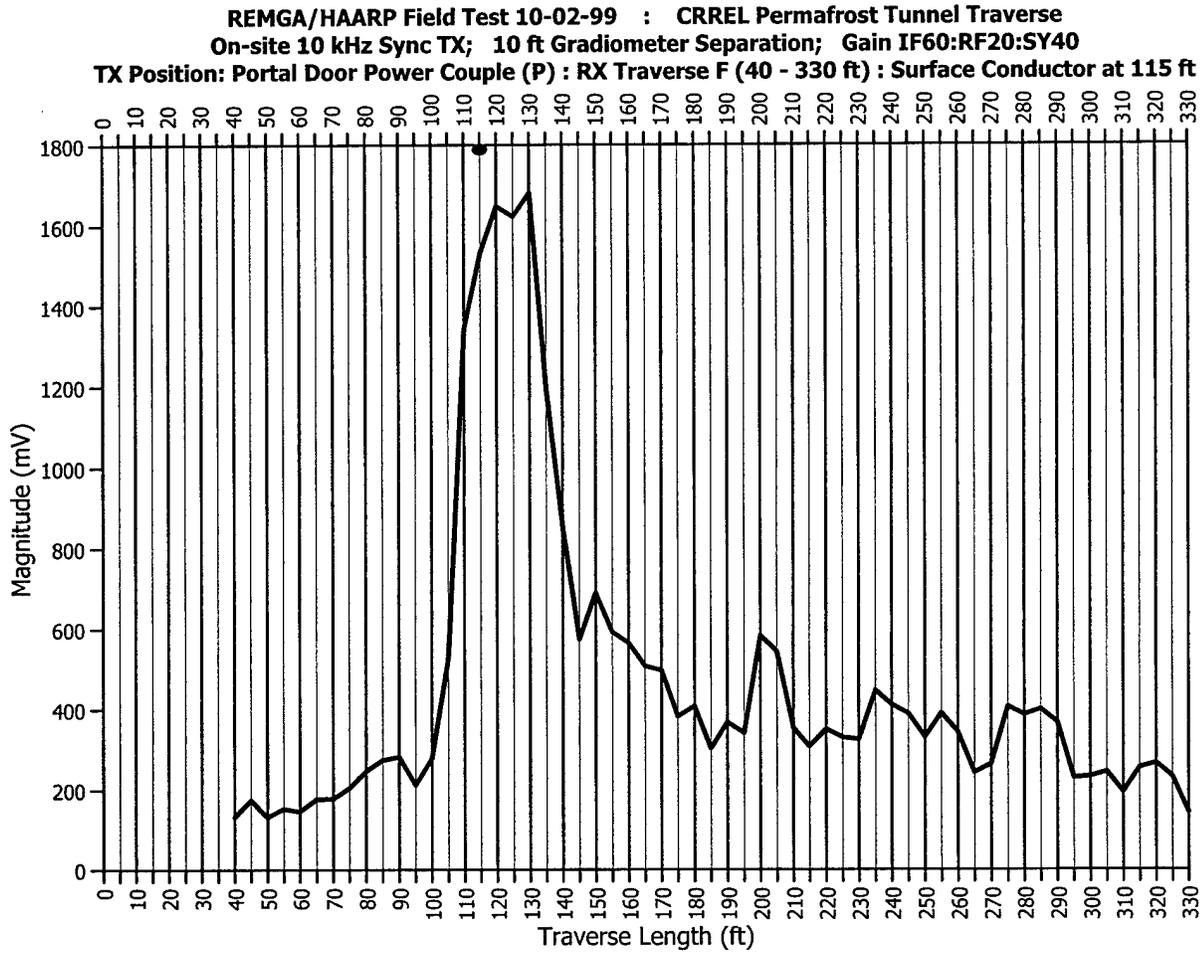
Figure 39. F traverse – EM gradiometer response versus traverse distance in feet

The surface cable predominates the response and a minimum response occurs in the Winze

Tunnel at 180 feet.

15.4 D Traverse

REMGA/HAARP Field Test 10-02-99 : CRREL Permafrost Tunnel Traverse
On-site 10 kHz Sync TX; 10 ft Gradiometer Separation; Gain IF60:RF20:SY40
TX Position: Portal Door Power Couple (P) : RX Traverse D (10 - 200 ft) : Surface Conductor at 120 ft
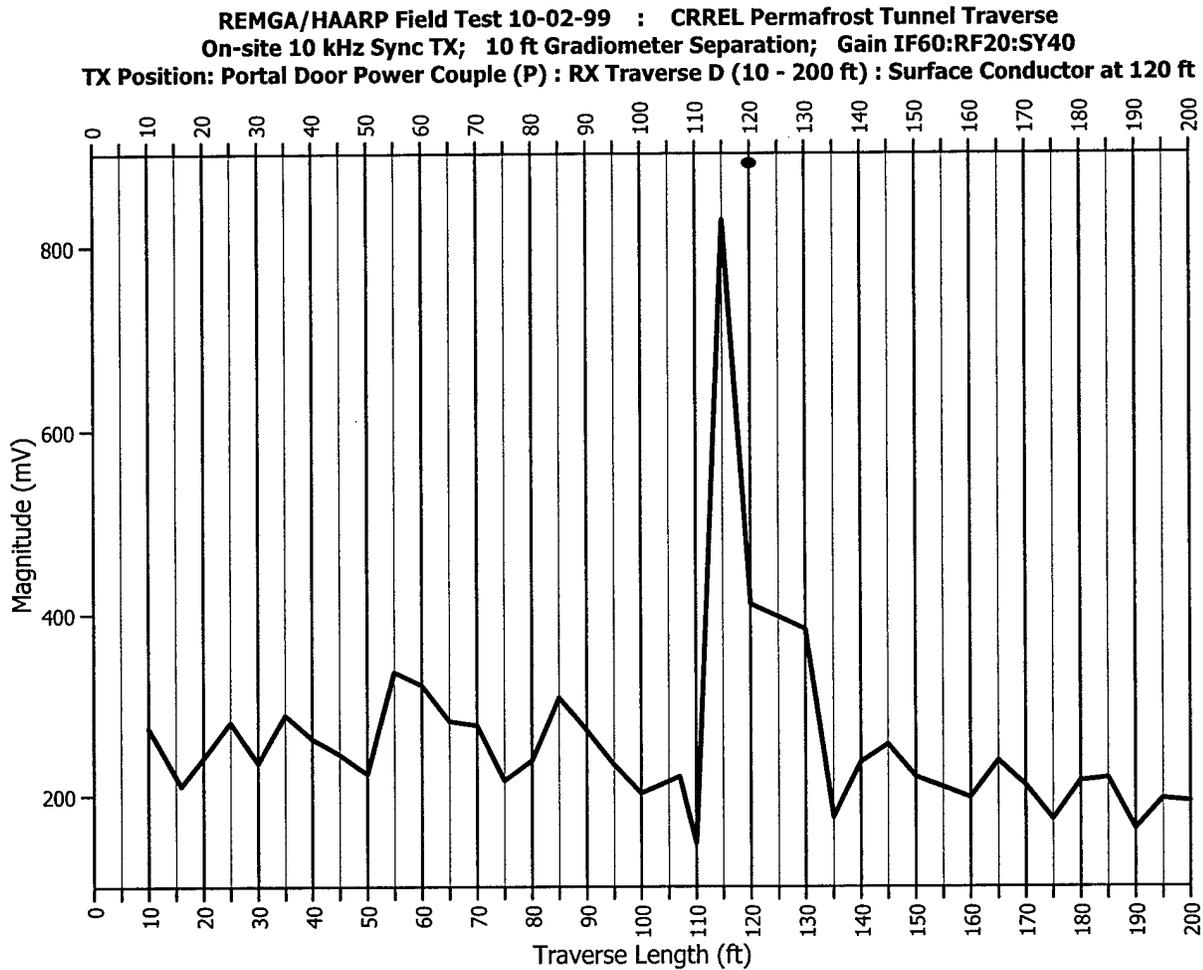
Figure 40. D traverse – EM gradiometer response versus traverse distance in feet

The surface power line response predominates the response.

15.5 E Traverse

REMGA/HAARP Field Test 10-02-99 : CRREL Permafrost Tunnel Traverse
On-site 10 kHz Sync TX; 10 ft Gradiometer Separation; Gain IF60:RF20:SY40
TX Position: Portal Door Power Couple (P) : RX Traverse E (100 - 130 ft) : Surface Conductor at 115 ft
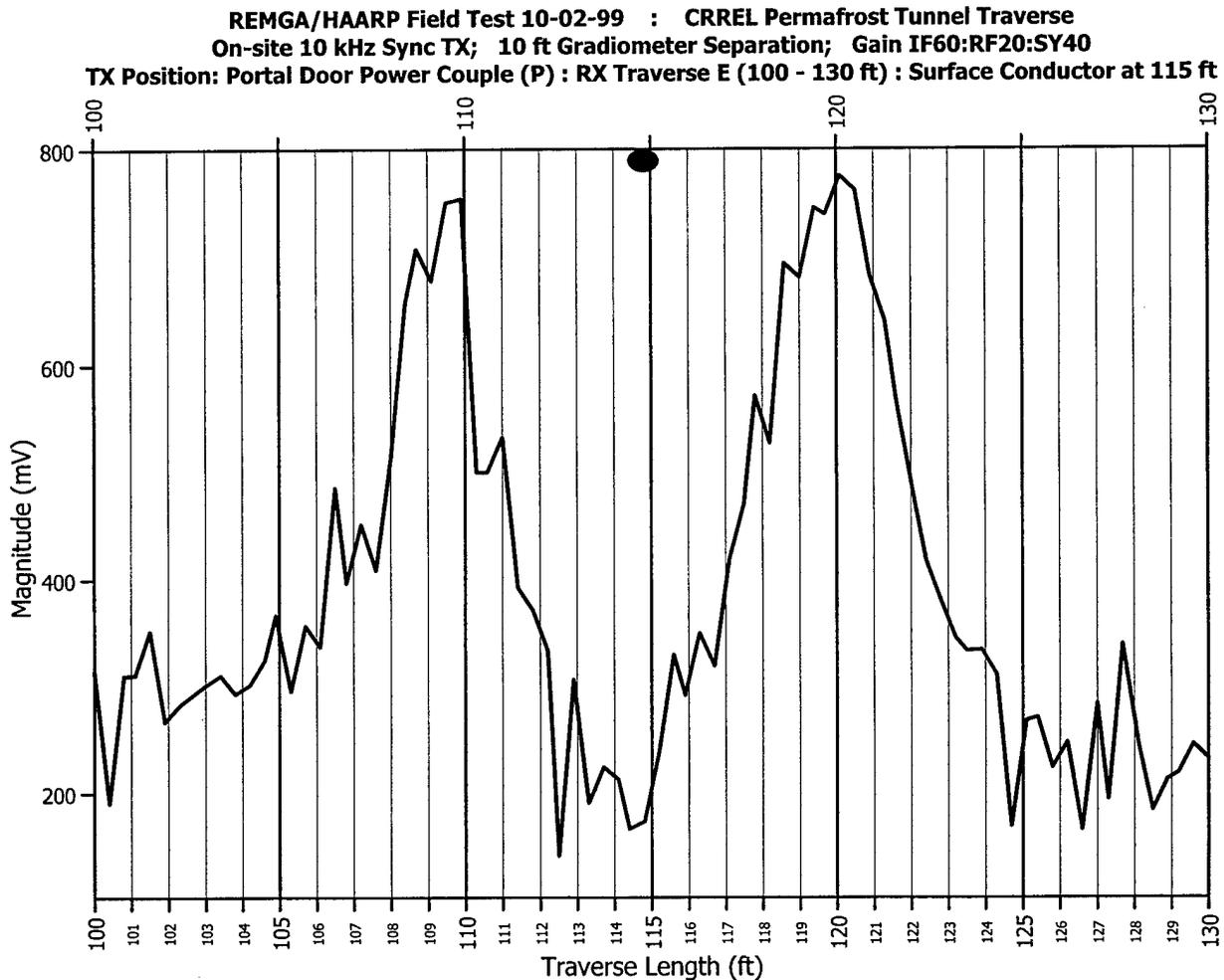
Figure 41. E scan – EM gradiometer with TX located scan C location

The induced current vanishes at the end of the passageway and ends an observable

gradiometer response, however, the combination surface cable and the shaft creates an anomaly

in the data.

16. CONCLUDING REMARKS AND RECOMMENDATIONS

Widespread knowledge and belief by Rogue Nation leaders that this nation's high-altitude

reconnaissance and stealth technologies can effectively destroy surface-based military assets has

caused the development of UGCs. These complexes enable the 20 or more Rogue Nations to counter the effectiveness of high-altitude reconnaissance/stealth technologies. To regain the capability of destroying the Rogue Nation leader's ability to wage war and support terrorist activities against his neighbors, UGC detection and imaging technology is urgently needed. This work has demonstrated that an EM gradiometer receiver can be self-synchronized to the primary wave illuminating a UGC, and by the action of the gradiometer antenna array suppress the primary wave so that the much smaller scattered wave from the UGC can be detected with a high S/N ratio. Further, the receiver synchronous detection process maximizes the receiver threshold detection sensitivity so that signals in the sub picoTesla range can be measured on the surface. By analyzing the collected data, the center line of passageways within the complex and burial depth has been determined.

The high threshold detection sensitivity of the synchronized EM gradiometer receiver enables HAARP EM waves to be used in the controlled simulation of other opportunistic earth-ionosphere waveguide standoff transmitters.

While the Navy low-frequency transmitter is a standoff source, it can not be used in evolutionary development, which requires a search for the optimum operational frequency to maximize the UGC S/N ratio. HAARP can be used for this purpose. Most of the HAARP research projects conducted to date have used modulation frequencies below 1,000 Hz. Equation (9) and Figure 9 teach that frequencies up to 10 kHz (which is still in a trial mode at the HAARP facility) may be optimum for the UGC detection problem. The magnitude of the emf magnetic dipole antenna output signal increases with ω, which allows EM gradiometer receivers with stable gain to be built. A 10-kHz sync EM gradiometer would achieve a factor of

---

Detection and Imaging of Underground Structures by Exploiting ELF/VLF Radiowaves
Final Report

20 improvement over a 500-Hz EM gradiometer. Much smaller gradiometer antenna arrays can be built at 10 kHz than can be built at 500 Hz. There appear to be modulation frequency bands where ionospheric noise reaches minimum values. HAARP modulation frequency would be changed so as to maximize the S/N over the Silver Fox Tunnel. Because the acquired sync EM gradiometer data result in a high S/N ratio, very little processing is necessary. The recording and logging standoff computer should include software code for real-time display of data. By incorporating a global positioning system (GPS) receiver into the sync EM gradiometer design, the data can be analyzed to determine burial depth. A series of experiments with the sync EM gradiometer receiver should be conducted during the Spring 2000 campaign. The demonstration would investigate which other standoff waveguide sources might be used to achieve coverage over the more than 20 Rogue Nations' UGC sites.

This project paves the way for development of UGC detection and imaging technology that can be deployed when access is denied. The sync EM gradiometer receiver should be developed so that it can be delivered to the site just prior to or during attack. The development of a penetrator-transponder (PT) reconfiguration of the sync EM gradiometer would be the goal of a future project. The idea of developing a magnetohydrodynamic device (MHDD) (chemical explosive-driven induction coil) that could be delivered just prior to or during attack would produce an effective primary EM wave illumination source. When the HMDD airblast ordnance is combined with an air drop PT, the UGC response information will be sent to the overhead satellite to provide information complex orientation, type of rock overlying the structure, and burial depth. Such information would be of use to mission planners.

REFERENCES

1. Freeman, L. E., and A. C. Cogbill. 1999. *A Catalog of Underground Detection Technology Test Sites.* Nonproliferation and National Security Office of R&D. Rpt. 10. DOE/NN/0003.

2. Middleton, David. 1987. *Introduction to Statistical Communication Theory.* Los Altos, California: Peninsula Publishing.

3. Summary Report *Evaluation of Additional Tunnel Detection Research Techniques at the California Tunnel Site.* 18 August–3 September 1993. U.S. Army Belvoir RD&E Center (BRDEC) Physical Security Equipment Division Geophysics Team.

4. Mahrer, K. D., and D. F. List. March–April 1995. "Radio Frequency Electromagnetic Tunnel Detection and Delineation at the Otay Mesa Site." *Geophysics,* Vol. 60, No. 2.

5. Benchmark study of technical capabilities, research efforts, and recommendations for underground target detection using geophysical techniques. 1994. US Department of Energy Report DOE/NN/001.

6. Bartel, L. C., D. H. Cress, and L. G. Stolarczyk. 1998. "Use of EM Gradiometer Concept for Detection of Underground Structures." *Journal of Environmental and Engineering Geophysics.* Vol. II, pp. 126–136.

7. Harrington, R. F. 1961. *Time –Harmonic Electromagnetic Fields,* pp. 233–234. New York: McGraw-Hill, Inc.

8. Stolarczyk, L. G. January 12–16, 1988. "Long Feature Tunnel Detection Methodologies using Phase Coherent Electromagnetic Instrumentation." Third Technical Symposium on Tunnel Detection Proceedings. Golden, Colorado.

9. Burrows, M. L. 1978. *Elf Communications Antennas.* Southgate House Stevenage, England: Peter Peregrins Ltd.

10. Hill, D. A. 1990. "Nearfield and Farfield Excitation of a Long Conductor in a Lossy Medium." Report NISTIR 3954 National Institute of Standards and Technology, Boulder, Colorado.

11. Stolarczyk, L. G. August 1991. "Emergency and Operational Low and Medium Frequency Band Radio Communications System for Underground Mines." *IEEE Transactions on Industry Applications,* Vol. 27, No. 4.

12. Cress, D. H., L. C. Bartel, B. Brock, D. L. Alumbaugh, and G. A. Newman. *Detection of Subsurface Structures using Electromagnetic Induction Techniques.* Sandia National Laboratories report, to be published.

REFERENCES (CONCLUDED)

13. Hill, D. A., and J. R. Wait. 1974. "Excitation of monofilar and bifilar modes on a transmission line in a circular tunnel." *J. Appl. Phys.,* vol. 45, pp. 3402–4356.

14. Hill, D. A. April 26–29, 1993. "Gradiometer Antennas for Tunnel Detection." Fourth Technical Symposium on Tunnel Detection Proceedings. Golden, Colorado.

15. Stolarczyk, L. G. April 26–29, 1993. "Gradiometer Antennas for Detection of Tunnels by Scattered Electromagnetic waves." Fourth Tunnel Detection Symposium on Subsurface Exploration Technology Proceedings. Golden, Colorado.

16. Kelly, Robert E. 26 April 1999. *Underground Structure Detection by Surface Magnetic Gradient Measurements.* Los Alamos National Laboratory. LDRD final report.